UNIVERSITY OF HELSINKI

https://helda.helsinki.fi

Which Extratropical Cyclones Contribute Most to the Transport of Moisture in the Southern Hemisphere?

Sinclair, V. A.; Dacre, H. F.

2019-03-16
American Geophysical Union
http://hdl.handle.net/10138/302090
Sinclair, V A & Dacre, H F 2019, 'Which Extratropical Cyclones Contribute Most to the Transport of Moisture in the Southern Hemisphere?', Journal of Geophysical Research : Atmospheres, vol. 124, no. 5, pp. 2525-2545. https://doi.org/10.1029/2018JD028766

Downloaded from Helda, University of Helsinki institutional repository. https://helda.helsinki.fi
This is an electronic reprint of the original article.
This reprint may differ from the original in pagination and typographic detail.
Please cite the original version.

Which extra-tropical cyclones contribute most to the transport of moisture in the Southern Hemisphere?

V. A. Sinclair,[1] and H. F. Dacre,[2]

Corresponding author: V. A. Sinclair, Institute for Atmospheric and Earth System Research / Physics, Faculty of Science, University of Helsinki, PO BOX 64, FI-00014, Finland (Victoria.Sinclair@helsinki.fi)

[1]Institute for Atmospheric and Earth System Research / Physics, Faculty of Science, University of Helsinki, Helsinki, Finland

[2]Department of Meteorology, University of Reading, Reading, UK

This article has been accepted for publication and undergone full peer review but has not been through the copyediting, typesetting, pagination and proofreading process which may lead to differences between this version and the Version of Record. Please cite this article as doi: 10.1029/2018JD028766

©2018 American Geophysical Union. All rights reserved.

Abstract. Predicted changes in Southern Hemisphere (SH) precipitation and Antarctic ice mass correspond to variations in the meridional moisture flux (MMF). Thirty-five years of ERA-Interim reanalysis data are combined with an extra-tropical cyclone (ETC) identification and tracking algorithm to investigate factors controlling SH MMF variability in the mid-latitudes and near Antarctica. ETC characteristics which exert the strongest control on ETC MMF are determined thus identifying which ETCs contribute most SH moisture transport. ETC poleward propagation speed exerts the strongest control on the ETC MMF across the Antarctic coastline. In SH winter, ETCs with the largest poleward propagation speeds transport 2.5 times more moisture than an average ETC. In the mid-latitudes, ETC genesis latitude and poleward propagation speed have a similar influence on ETC MMF. Surprisingly, ETC maximum vorticity has little control on ETC MMF. Cyclone compositing is used to determine the reasons for these statistical relationships. ETCs generally exhibit a dipole of poleward and equatorward MMF downstream and upstream of the cyclone centre respectively. However, ETCs with the largest poleward propagation speeds resemble open frontal waves with strong poleward moisture transport downstream of the cyclone centre only and thus result in the largest MMF. These results suggest that inhomogeneous trends and predicted changes in precipitation over Antarctica may be due to changes in cyclone track orientation, associated with changes to the large-scale background flow, in addition to changes in cyclone number or intensity.

©2018 American Geophysical Union. All rights reserved.

Accepted Article

Accepted Article

1. Introduction

Atmospheric water vapor plays a fundamental role in determining the state of the Earth's climate. Water vapor is a powerful greenhouse gas and thus its distribution influences global temperature patterns. Furthermore, the spatial distribution of water vapor, and in particular the convergence of water vapor, is strongly correlated with precipitation patterns. However, water vapor is distributed inhomogeneously across the globe. Typically the atmospheric moisture content is largest at the equator and near the surface and smallest at the poles and in the upper troposphere due to the Clausius-Clapeyron equation (which determines the water holding capacity of the atmosphere and predicts an increase of 7% for every 1°C rise in temperature). However, the atmospheric circulation transports moisture meridionally and vertically resulting in complex spatial patterns and intrusions of moist air into the mid and high latitudes and mid to upper troposphere.

To identify which aspects of the circulation are most important in the meridional transport of moisture, the flow can be decomposed into the mean meridional circulation, stationary eddies and transient eddies. *Tietäväinen and Vihma* [2008] and *Tsukernik and Lynch* [2013] applied this traditional flow decomposition method to ERA-40 and ERA-Interim data respectively. *Tietäväinen and Vihma* [2008] showed that 85% of the total poleward moisture transport at 60°S is due to transient eddies, whereas using the newer reanalysis *Tsukernik and Lynch* [2013] found that transient eddies were responsible for 81% of the total moisture transport at 60°S. Transient eddies, deviations from the zonal and temporal mean, include extra-tropical cyclones (ETCs). Therefore, changes to either the number or location of ETCs is likely to alter the poleward moisture transport and

©2018 American Geophysical Union. All rights reserved.

precipitation patterns in the mid and high latitudes. Many studies have considered how the storm tracks are likely to change in the future in both the northern and southern hemispheres [e.g. *Fyfe*, 2003; *Wang and Swail*, 2006]. However, precipitation patterns could also change if the variability of extra-tropical cyclones and the amount of moisture transported by an ETC changes even if the number of ETCs remains the same.

Changes to moisture transport by ETCs in the Southern Hemisphere (SH) potentially could have major impacts. The Antarctic ice sheet is the largest potential source of future sea level rise due to its large mass [*Schoen et al.*, 2015]. Variability in Antarctic ice mass is determined by the balance between precipitation accumulation over the continent and mass loss due to melting, sublimation and ice calving [*Bromwich*, 1990; *Davis et al.*, 2005; *Seo et al.*, 2015; *Roberts et al.*, 2015]. Since a large fraction of the precipitation in Antarctica is associated with ETCs, changes in ETC number and moisture transport that result in a changed distribution of precipitation will be important for future Antarctic ice mass [*Noone et al.*, 1999; *Papritz et al.*, 2014; *Altnau et al.*, 2015]. There is evidence to suggest that only a few ETCs are responsible for the majority of the precipitation over Antarctica, particularly in the interior of the continent [*Bromwich*, 1988; *Krinner et al.*, *Gorodetskaya et al.*, 2014]. This motivates an investigation of what factors lead to the greatest variability in the amount of moisture an ETC can transport polewards.

The structure of ETCs has been extensively studied and conceptual cyclone models developed [e.g. *Bjerknes and Solberg*, 1922; *Shapiro and Keyser*, 1990]. *Carlson* [1980] presented the conveyor belt cyclone model which includes three main air streams: a warm conveyor belt (WCB), a cold conveyor belt (CCB) and the dry intrusion. The WCB originates in the boundary layer, ascends and moves polewards. Although the conceptual

©2018 American Geophysical Union. All rights reserved.

Accepted Article

models have been developed primarily based on northern hemisphere (NH) observations, studies indicate that ETCs in the SH do not differ significantly from those occurring in the NH. For example, *Field and Wood* [2007] compared ETCs in the North Atlantic, North Pacific, South Atlantic and South Pacific using satellite data and concluded that the cloud and precipitation properties of ETCs with a given strength and water vapor path are similar in all ocean basins. Furthermore, *Govekar et al.* [2011] created three-dimensional composites of southern hemisphere extra-tropical cyclones using satellite and reanalysis data and concluded that the structure of SH ETCs agrees well with conceptual models with both the warm conveyor belt and dry intrusion being evident in their composites.

The poleward transport of moisture is determined by the water vapor content of the atmosphere and the meridional wind velocity. As atmospheric moisture content is largest at the equator and smallest at the poles, poleward moving airflows, such as the WCB, generally result in a poleward transport of moist air and equatorward moving airflows (e.g. the CCB and dry intrusion) an equatorward transport of drier air. Within ETCs the meridional wind velocity is the sum of the meridional velocity of the airflows within the ETC (ETC-relative airflows) and the meridional velocity of the ETC itself (ETC propagation velocity). The poleward airflow in ETCs is concentrated in the ascending moist warm conveyor belt whilst the equatorward airflow occurs in the descending dry intrusion airflow behind the cold front (Figure 1a). As the warm conveyor belt originates at lower altitudes and closer to the equator than the dry intrusion, the net ETC-relative meridional moisture flux (MMF) usually contributes a poleward component to the total MMF associated with ETCs. This suggests that more intense ETCs, with stronger ETC-relative winds, will transport more moisture polewards than weaker ETCs. The ETC

©2018 American Geophysical Union. All rights reserved.

Accepted Article

propagation velocity on the other hand can result in either a poleward or an equatorward MMF contribution to the total MMF associated with ETCs depending on their direction of travel. Thus ETCs with more meridional tracks (large poleward propagation velocity) are likely to transport more moisture polewards than those with more zonal tracks (smaller poleward propagation velocity, Figure 1b). Finally, ETCs generated at low-latitudes may transport more moisture polewards than those generated at high-latitudes due to higher atmospheric moisture content at their genesis locations (Figure 1c) and along the tracks that they subsequently follow.

The primary aim of this paper is to identify the synoptic-scale ETCs that contribute the greatest amount to meridional moisture flux variability. This is achieved by analyzing the relationships between ETC genesis latitude, intensity, meridional propagation velocity, and the MMF. The second aim is to quantify how the spatial pattern of MMF varies between ETCs with different genesis latitude, intensity, meridional propagation velocity and how the net MMF varies at different stages of the ETC development. This second aim is achieved by creating composites of ETC MMF.

The structure of this paper is as follows. The reanalysis data used in this study along with the methods are described in section 2. A climatology of the zonal mean total MMF and ETC MMF is shown in section 3 before the main results are presented in sections 4 and 5. The conclusions are presented in section 6.

2. Data and Method

This study utilizes 35 years of ERA-Interim reanalysis data from 1979 to 2013. ERA-Interim data has a spatial resolution of approximately 80 km (T255 spectral) and a temporal resolution of 6 hours, allowing the evolution of synoptic-scale weather systems to

©2018 American Geophysical Union. All rights reserved.

Accepted Article

be captured. Pressure level data, with a vertical resolution of 25 hPa between 1000 hPa and 700 hPa and 50 hPa between 700 hPa and 300 hPa, are analyzed.

From ERA-Interim, the tracks of all ETCs in the SH (0 - 90°S) are identified using an objective feature tracking algorithm, TRACK ([*Hodges*, 1994, 1995]) which has been applied in numerous previous studies [e.g. *Hoskins and Hodges*, 2005; *Jung et al.*, 2012; *Zappa et al.*, 2013]. TRACK identifies localized cyclonic maxima in the 850-hPa relative vorticity (positive in the Northern Hemisphere and negative in the Southern Hemisphere). Before the tracking is performed, the large-scale background field is removed from the full relative vorticity field by setting the coefficients for total wavenumbers less than or equal to five to zero. Small scale noise and mesoscale variability is also removed by truncating the relative vorticity to T42 spectral resolution which ensures that only synoptic-scale extra-tropical cyclones are identified. The output from TRACK consists of the longitude, latitude and relative vorticity of each point (every 6 hours) along each ETC track from genesis to lysis. Thus, one complete track is considered as one ETC. From this output, the genesis latitude, maximum intensity and the average poleward propagation speed between the time of genesis and the time of maximum intensity is calculated for each track / ETC. Initially all localized cyclonic vorticity maximas between the equator and south pole are identified and tracked, however, those which remain north of 30°S for their entire life time are excluded from the analysis as they are likely tropical, not extra-tropical, cyclones. Furthermore, only ETCs which have cyclonic relative vorticity values exceeding 1×10^{-5} s^{-1} are retained. Finally the tracks are filtered to remove stationary or short-lived ETCs; only tracks which are at least 1000 km long and last for at least 2 days are retained. The tracks are available from zenodo [*Sinclair and Dacre*, 2019].

©2018 American Geophysical Union. All rights reserved.

Accepted Article

The total vertically integrated meridional moisture flux, $\mathrm{MMF}_{\mathrm{TOT}}$, is also calculated from ERA-Interim and is given by

$$\mathrm{MMF}_{\mathrm{TOT}} = -\frac{1}{g}\int_{p1}^{p2}(vq)dp \tag{1}$$

where v is the meridional wind component, q is the specific humidity, g is the gravitational constant, p_1 is 1000 hPa and p_2 is 300 hPa. The negative sign is introduced so that poleward moisture transport in the southern hemisphere is defined to be be positive. The MMF from lower-latitudes can be used as a proxy for precipitation [*Tsukernik and Lynch*, 2013] which is particularly useful over the Antarctic continent as ERA-Interim precipitation is not very reliable over the interior of Antarctica due to the limited number of assimilated observations such as radiosonde humidity profiles.

2.1. Masking approach

To calculate the vertically integrated meridional moisture flux due to ETCs ($\mathrm{MMF}_{\mathrm{ETC}}$), the ETC tracks are combined with a masking method. We follow *Hawcroft et al.* [2012] and assume that the area influenced by an ETC is given by a circle of constant radius centered on the localized cyclonic vorticity maximas identified by TRACK. Thus, an "ETC mask" is calculated for each time step where the regions influenced by an ETC are given a value of one (i.e. they are inside the ETC mask) and regions that are not influenced are given a value of zero (i.e. they are outside the ETC mask). $\mathrm{MMF}_{\mathrm{ETC}}$ is then calculated by

$$\mathrm{MMF}_{\mathrm{ETC}} = \mathrm{MMF}_{\mathrm{TOT}} \times mask. \tag{2}$$

This ETC tracking and masking approach allows the MMF due to certain subsets of ETCs, e.g. those with certain characteristics, to be calculated. In this study, ETCs are subset based on their maximum intensity, genesis latitude and meridional propagation

©2018 American Geophysical Union. All rights reserved.

Accepted Article

velocity. For each variable, six bins were created (see Table 1). However, the tracking and masking approach does have disadvantages, one of which is the assumption that ETCs have a constant radius. *Rudeva and Gulev* [2007] showed that cyclone radius (calculated to be where the first radial derivative of SLP becomes zero) varies during the cyclone life cycle and can vary from 300 km over continents to more than 900 km over oceans. Here we use a constant radius of 12 degrees except in DJF (southern hemisphere summer) when a radius of 11 degrees is used. These values were selected based on previous studies [e.g. *Tsumi et al.*, 2016; *Hawcroft et al.*, 2012; *Zappa et al.*, 2015] and by visually examining composite cyclones. The sensitivity of ETC MMF to the choice of radius was investigated (Figure 2). As expected, increasing the radius from 8 to 12 degrees increases the amount of MMF_{ETC}. Changing the radius does not alter the latitude of the maximum MMF_{ETC} nor how MMF_{ETC} varies with latitude. The sensitivity of the results to the choice of radius (R) is considered further in sections 3 and 4, however, the choice of radius does not affect the main conclusions of this study.

2.2. Cyclone composite approach

The masking approach has the advantages that all ETCs can be easily included in the analysis and that it is simple to determine the MMF due to ETCs across any given latitude. However, disadvantages of this approach include that all stages of ETCs are considered together (i.e intensification and decay) and that the spatial pattern of MMF relative to the center of a ETC cannot be determined. Thus, to complement the masking approach, a cyclone compositing approach is also taken. We follow the method previously used by *Catto et al.* [2010] and *Dacre et al.* [2012] to create cyclone composites of the meridional moisture flux (MMF), total column water vapor (TCWV) and mean sea level

©2018 American Geophysical Union. All rights reserved.

Accepted Article

pressure (MSLP). First, the ETC tracks identified by TRACK that are to be included in each composite are selected. Following a similar approach to *Rudeva and Gulev* [2011], who created cyclone composites for subsets of North Atlantic cyclones based on their intensity and lysis regions, we create composites for each of our bins (Table 1). For each composite 200 individual ETCs are selected from the "top" end of each bin. For example, for the speed bin 0 - 2 degrees per day, all ETCs in this bin are identified and ordered in terms of their speed and the top 200 from this bin (i.e. the fastest moving ETCs) are then selected to create the composite from. Cyclones were selected from the top of each bin to make sure that the composites had limited variability in terms of the predictor variable. Second, the position of each ETC at different offset times relative to the time of maximum vorticity are determined. Five different offset times are considered: 48 and 24 hours before the time of maximum intensity, the time of maximum intensity and 24 and 48 hours after the time of maximum intensity. Composites are created for each offset time. Third, a radial coordinate system with a radius of 12 degrees (11 degrees in DJF) is defined and centered on each cyclone center at each offset time. MMF, TCWV, and MSLP from ERA-Interim gridded fields are then interpolated onto this radial grid. Finally, to reduce smoothing errors, the cyclones are rotated so that all travel due east and then the MMF, TCWV and MSLP on the radial grid are averaged. The composite ETC is the simple arithmetic mean of the 200 individual, rotated ETCs.

3. Climatology of Total and ETC Meridional Moisture Flux

We represent the zonally averaged MMF by $\overline{MMF}$, where the over bar denotes a zonally averaged quantity. $\overline{MMF_{TOT}}$ varies between seasons (Figure 3a). Between 40 and 50°S, $\overline{MMF_{TOT}}$ is largest in March-April-May but at 65°S (approximately at the Antarc-

©2018 American Geophysical Union. All rights reserved.

Accepted Article

tic coastline), the largest values of $\overline{MMF_{TOT}}$ occur in June-July-August (JJA) despite the atmospheric moisture content being smallest in JJA. This JJA maximum can be explained by considering the moisture transported by ETCs: at 65°S, $\overline{MMF_{ETC}}$ is largest in JJA (7.37 kg $m^{-1}s^{-1}$ if R=8 degrees; 11.7 kg $m^{-1}s^{-1}$ if R=12 degrees) and smallest in December-January-February (DJF, 5.2 kg $m^{-1}s^{-1}$ if R=8 degree; 7.9 kg $m^{-1}s^{-1}$ if R=12 degrees). This seasonal variation in $\overline{MMF_{ETC}}$ is because in DJF and MAM the storm track is more zonal and closer to the pole than in JJA and September-October-November (SON) [*Hoskins and Hodges*, 2005]. In JJA and SON the storm track is more asymmetric with a spiral from the Atlantic and Indian Oceans towards Antarctica [*Williams et al.*, 2007]. Thus, despite the atmospheric moisture content being largest in DJF, the maximum moisture transport to the Antarctic coastline occurs in JJA due to the increased number of ETCs that cross 65°S. In all 35 years of data, 3944 ETC tracks cross the 65°S latitude circle in JJA compared to 2698 in DJF.

The percentage of MMF due to ETCs depends strongly on what radius is selected. At 50°S in JJA, assuming radii of 8, 10, 11 and 12 degrees, ETCs are identified as being responsible for 49%, 67%, 74% and 81% of the $\overline{MMF_{TOT}}$. The corresponding values in DJF are 54%, 72%, 79% and 85% respectively (Figures 3a and 3b).*Rudeva and Gulev* [2011] noted that ETCs in the North Atlantic, on average, do not have air-sea turbulent fluxes associated with them which are climatologically excessive once the ratio of the area affected by an ETC is compared to the total area. To ascertain if a similar result exists in terms of MMF, we determine if the areas influenced by extra-tropical cyclones have much greater MMF per unit area than those areas not influenced by an ETC. Two ratios are calculated: the ratio of the ETC-related MMF to the total MMF and the ratio

©2018 American Geophysical Union. All rights reserved.

Accepted Article

of the number of grid points affected by an ETC to the total number of grid points. For both ratios a radius of 12 degrees was used for JJA and 11 degrees for DJF. We then compare these two ratios. In JJA at 60°S, ETCs are responsible for 83% of the total MMF (assuming R=12 degrees) while ETCs influence 81% of grid points at 60°S (Figures 3c). In DJF (assuming R=11 degrees), the respective values are 85% and 75% (Figures 3d). Thus, ETCs are only responsible for slightly more meridional moisture transport than what would be expected in a climatological sense. However, if only poleward moving ETCs are considered, ETCs are responsible for 84% of the total MMF in JJA yet only influence 60% of grid points. In DJF, poleward moving ETCs are responsible for 91% of the total MMF but influence only 58% of grid points. It is thus apparent that equatorward moving ETCs contribute negatively to the net ETC-related MMF in DJF, and contribute very little to the net ETC-related MMF in JJA. If only ETCs which move polewards between the time of genesis and time of maximum intensity are considered, as is the case in the remainder of this paper, then it can be concluded that ETCs contribute more to the net poleward moisture transport than would be expected based on the ratio of the area affected by an ETC to the total area.

4. Characteristics of ETCs

Is it just the number of ETCs that control the $\overline{MMF_{ETC}}$ or do the characteristics of individual ETCs play a role in determining how much moisture is transported polewards in the southern hemisphere? To answer this question we normalized the sum of MMF_{ETC} at each grid point calculated over all time steps in each season by the sum of the mask counts at each grid point (i.e. the number of times a grid point has been affected by a

©2018 American Geophysical Union. All rights reserved.

Accepted Article

ETC),

$$|MMF_{ETC}| = \frac{\sum MMF_{ETC}}{\#masks}, \quad (3)$$

obtain $|MMF_{ETC}|$ where the vertical bars denote the average MMF per ETC. The zonal mean of this quantity is represented by $\overline{|MMF_{ETC}|}$. We now focus only on two seasons: JJA and DJF.

4.1. ETC Genesis Latitude

Figure 4 shows how $\overline{|MMF_{ETC}|}$ varies with ETC genesis latitude in both JJA and DJF in the mid-latitudes (50°S, Figure 4a) and near the Antarctic coastline (65°S, Figure 4b). In JJA at both 50° and 65°S there are large regression (Table 2) and correlation coefficients (Table T1 in supporting material) significant at the 99% level, indicating strong linear relationships between 90 - genesis latitude (i.e. distance from the pole) and $\overline{|MMF_{ETC}|}$. The large slope shown in Figure 4 therefore demonstrates that genesis latitude contributes considerably to the variability in $\overline{|MMF_{ETC}|}$. This result is not sensitive to the choice of radius (Figure S1 in supporting material). Thus, in southern hemisphere winter (JJA) ETCs forming closer to the equator lead to more poleward moisture flux than those forming further poleward, likely because ETCs generated nearer the equator usually form in and track through a moister environment. In DJF, there is also a strong positive linear relationship between 90 - genesis latitude (i.e. distance from the pole) and $\overline{|MMF_{ETC}|}$ but unlike in JJA, this correlation only exists in the mid-latitudes. In DJF, the linear regression coefficients between 90-genesis latitude and $\overline{|MMF_{ETC}|}$ poleward of 65° are not statistically significant (Table 2) and the correlation coefficients are less than 0.65.

Figures 5a–c and 6a–c show the spatial pattern of the relationship shown in Figure 4. In Figures 5 and 6 blue colors indicate that ETCs in that subset have smaller $|MMF_{ETC}|$ than

©2018 American Geophysical Union. All rights reserved.

Accepted Article

average whilst red colors indicate that they have larger $|MMF_{ETC}|$ than average. Average $|MMF_{ETC}|$ is due to all poleward traveling cyclones at each grid point (i.e. those ETCs which moved equatorward between the time of genesis and time of maximum intensity were excluded). In general $|MMF_{ETC}|$ is greater for ETCs generated at lower latitudes but the relationship between $|MMF_{ETC}|$ and ETC genesis latitude is not zonally homogeneous and varies between seasons (Figures 5a-c, 6a–c). In JJA and DJF there is a strong relationship between genesis latitude and $|MMF_{ETC}|$ in Pacific sector between 140°W and 60°W, which is shifted poleward in JJA compared to in DJF. A strong relationship is also present in the Indian Ocean between 90°E and 120°E in JJA and slightly more to the west in DJF - between 60°E and 90°E. In particular, ETCs generated north of 45°S (Figure 5c, 6c) appear important for transporting moisture onto the coastal areas of East Antarctic. This is consistent with Lagrangian back trajectory studies which show that Antarctic precipitation is dominated by moisture from a subtropical/mid-latitude band [*Delaygue et al.*, 2000; *Sodemann and Stohl*, 2009]. In contrast, in the Ross Sea and in the Weddell Sea there is little relationship between genesis latitude and $|MMF_{ETC}|$ in either JJA or DJF.

4.2. ETC Relative Vorticity

Figure 4 also shows how $\overline{|MMF_{ETC}|}$ varies with ETC maximum 850-hPa cyclonic relative vorticity. At 50°S the regression coefficient between ETC maximum cyclonic relative vorticity and $\overline{|MMF_{ETC}|}$ in DJF is 4.31 kg $m^{-1}s^{-1}$ showing that relative vorticity leads to a small amount of variability in $\overline{|MMF_{ETC}|}$. Moreover, the corresponding correlation coefficient is 0.86 and significant at the 95% level (Table T1 in supporting material). In JJA, there is no statistically significant correlation between ETC maximum cyclonic rela-

©2018 American Geophysical Union. All rights reserved.

Accepted Article

tive vorticity at 50°S demonstrating that ETC maximum cyclonic vorticity does not lead to any variability in $\overline{|MMF_{ETC}|}$

At 65°S, the regression coefficient (correlation coefficient) between ETC maximum cyclonic relative vorticity and $\overline{|MMF_{ETC}|}$ in JJA is 2.21 kg m^{-1}s^{-1} (0.97) (Tables 2 and T1 in supporting material) showing that near the Antarctic coastline stronger ETCs transport more moisture polewards than weaker ETCs. Similar statistically significant positive correlations are also observed at 55 and 60°S in JJA. However, in DJF, poleward of 60°S there is no correlation between ETC maximum cyclonic relative vorticity and $\overline{|MMF_{ETC}|}$ and the regression coefficients are small or negative. Figure 4 and Table 2 also demonstrate that maximum cyclonic vorticity has a weaker relationship with $\overline{|MMF_{ETC}|}$ than either genesis latitude or poleward propagation speed in both seasons. This result is also not dependent on the choice of radius (Figure S1 in supporting material). Therefore, it could be concluded that maximum intensity of ETCs, as measured by cyclonic relative vorticity, contributes very little to the variability in $\overline{|MMF_{ETC}|}$ and thus has little impact on the moisture flux towards and onto the Antarctic continent. However, the lack of a strong correlation in the zonal mean may be due to spatial variations.

Figures 5d–f and 6d–f show the spatial pattern of the relationship shown in Figure 4. In general the weakest ETCs (Figure 5d) contribute below average $|MMF_{ETC}|$, but this is confined to the southern Atlantic and Indian Oceans and is only evident in JJA. Even in JJA, the strongest ETCs (Figure 5f) only contribute above average $|MMF_{ETC}|$ in very few areas confirming that the relationship between ETC intensity and $|MMF_{ETC}|$ is weak and non-existent in some locations. In addition, in the Weddell Sea stronger ETCs contribute below average MMF in both JJA and DJF, which is opposite to our hypothesis. The

©2018 American Geophysical Union. All rights reserved.

Accepted Article

Weddell Sea is a meteorologically complex area due to the occurrence of both katabatic and barrier winds and lee side cyclogenesis. Potentially the negative correlation between ETC maximum vorticity and MMF in this region is due to the strong horizontal pressure gradients associated with intense ETCs which draw in cold continental air on their western side and enhance the equatorward katabatic winds [*Parish and Bromwich*, 1998; *Orr et al.*, 2014] and thus reduce the total ETC-related MMF in this region.

4.3. ETC Poleward Propagation Speed

Figure 4 shows how $\overline{|MMF_{ETC}|}$ varies with ETC poleward propagation speed. Strong relationships are evident at both 50 and 65°S and in both JJA and DJF, however for the same latitude the regression coefficients are larger in DJF than in JJA suggesting that ETC poleward propagation speed leads to more variability in $\overline{|MMF_{ETC}|}$ in SH summer than winter. This is consistent with *Pfahl et al.* [2014] who used Lagrangian backward trajectories to show that moisture transport in summer has a more pronounced meridional component than in winter. At 50°S, the regression coefficient is 27.54 kg $m^{-1}s^{-1}$ in JJA and 37.99 kg $m^{-1}s^{-1}$ in DJF which is a much stronger relationship than was found between ETC maximum vorticity and $\overline{|MMF_{ETC}|}$ at 50°S but slightly weaker than found between genesis latitude and $\overline{|MMF_{ETC}|}$. This indicates that in the mid-latitudes $|MMF_{ETC}|$ is most strongly influenced by the genesis latitude of the ETC but that ETC propagation speed is also important. At 65°S, the regression coefficient is 7.86 kg $m^{-1}s^{-1}$ in JJA and 10.96 kg $m^{-1}s^{-1}$ in DJF, both of which are stronger relationships than were found for either the ETC genesis latitude or maximum vorticity. Thus, near the Antarctic coastline $|MMF_{ETC}|$ is most strongly influenced by propagation speed of the ETC. This relationship between ETC propagation speed and $\overline{|MMF_{ETC}|}$ likely exists because the moisture flux

©2018 American Geophysical Union. All rights reserved.

Accepted Article

due to fast moving ETCs may be dominated by the moisture evaporated at the ETC genesis location whereas slower moving ETCs likely depend more on moisture acquired along their track which will be less than that available at their more equatorward genesis locations. As a result, fast moving ETCs have a much larger poleward MMF than slow moving ETCs.

The strong relationship between poleward propagation speed and MMF is fairly spatially homogeneous (Figure 5g–i) in JJA suggesting that the ETC poleward propagation speed is universally important for determining $|MMF_{ETC}|$. In DJF, there is more spatial variability, with the strongest relationship observed in the south Atlantic. ETCs with large poleward propagation speeds typically results in 2.5 (i.e. $\log_{10}(2.5) = 0.39$) times the average $|MMF_{ETC}|$. The SH extra-tropical storm track is more asymmetric in winter (JJA) than in summer (DJF), with a spiral from the Atlantic and Indian Oceans towards Antarctica [*Hoskins and Hodges*, 2005]. This is confirmed when the mean poleward propagation speed of poleward moving ETCs is considered. In JJA, poleward moving ETCs have a mean poleward propagation speed of 3.87 degrees latitude by day whereas in DJF the mean value is 3.46 degrees per day. Normalized histograms (not shown) also demonstrate that a larger percentage of ETCs in JJA have large poleward propagation speeds than in DJF: 8.3% of ETCs have a poleward propagation speed greater than 8 degrees per day in JJA but only 5.3% do in DJF. This seasonal change in track orientation is thus very important for determining the seasonal differences in poleward MMF and precipitation in high latitudes and over the Antarctic continent.

©2018 American Geophysical Union. All rights reserved.

Accepted Article

4.4. Multiple linear regression

The results shown in Figure 4 and Table 2 are based on three independent linear regressions which were conducted between $\overline{|MMF_{ETC}|}$ and each predictor variable (maximum cyclonic vorticity, poleward propagation speed and 90-genesis latitude). Weak but statistically significant linear relations exist between the different predictor variables. Therefore, to determine if the interaction between the predictors significantly affects the linear relationships shown in Figure 4, multiple linear regression between the three predictors and $\overline{|MMF_{ETC}|}$ at 50°S and 65°S is performed.

Rather than dividing the data into bins and thus having a sample size of 6 as was the case for the simple linear regression, here each time step is considered as one sample resulting in a sample size of 12280 for JJA and 12636 for DJF. First, for each time step all ETCs which could contribute to $\mathrm{MMF_{ETC}}$ at either 50°S or 65°S are identified. In JJA, as the radius of the ETC mask is 12 degrees, this is all ETCs with their center located between 38°S and 62°S for $\mathrm{MMF_{ETC}}$ at 50°S and between 53°S and 77°S for $\mathrm{MMF_{ETC}}$ at 65°S. In DJF, since the radius is 11 degrees, for $\mathrm{MMF_{ETC}}$ at 50°S this is all ETCs with their center between 39°S and 61°S and between 54°S and 76°S for $\mathrm{MMF_{ETC}}$ at 65°S. The maximum cyclonic vorticity, mean poleward propagation speed between the time of genesis and time of maximum intensity, and the genesis latitude were obtained for each of these ETCs. So that ETCs closer to the latitude of interest (i.e. 50°S or 65°S) are more strongly weighted than those further away, the predictor values were weighted by the ratio of the length of the chord of the ETC mask which lies along the relevant latitude circle to the maximum ETC mask diameter (22 or 24 degrees). Thus, the weighted predictor

©2018 American Geophysical Union. All rights reserved.

Accepted Article

values ($P_{weighted}$) are given by

$$\mathrm{P_{weighted}} = P \times \frac{2\sqrt{(R^2 - a^2)}}{2R} \tag{4}$$

where P is the predictor variable, R is the radius of the ETC mask (11 or 12 degrees) and a is the distance in degrees between the center of the ETC and latitude of interest. For each time step, the mean value of each weighted predictor values is calculated. Note that this is not a zonal mean as there are many points with no ETCs present, but rather a mean of the ETCs which influence the MMF at either 50 or 65°S at each time. Multiple linear regression is then performed using the weighted mean predictor variables centered on their mean values and normalized by their standard deviations and $\overline{|\mathrm{MMF_{ETC}}|}$ at 50°S and 65°S.

The multiple linear regression results (Table 3) in general support the results obtained from the simple linear regression. Poleward propagation speed is now identified to be the most important ETC characteristic influencing how much moisture a given ETC can transport poleward; at both 50 and 65°S and in both JJA and DJF, speed has the largest regression coefficient and smallest p-value (not shown). This differs slightly from the the results of the simple linear regression where genesis latitude contributed the most to $\overline{|\mathrm{MMF_{ETC}}|}$ variability in the mid-latitudes. In JJA, the multiple linear regression indicates that genesis latitude is the second most important ETC characteristic influencing variability in MMF. However, in contrast to the results from the simple linear regression, the multiple linear regression indicates that ETC maximum vorticity does have a role in influencing $|\overline{MMF_{ETC}}|$. At 50°S, in both JJA and DJF, there is a positive statistically significant regression coefficient between $|\overline{MMF_{ETC}}|$ and ETC maximum vorticity. A more complex situation emerges at 65°S. In JJA only the interaction term between max-

©2018 American Geophysical Union. All rights reserved.

Accepted Article

imum vorticity and genesis latitude has a significant regression coefficient demonstrating that maximum vorticity is not a dominant factor influencing moisture transport at the Antarctic coastline in SH winter. In contrast in DJF there is a statistically significant negative regression coefficient between ETC maximum vorticity and $|\overline{MMF_{ETC}}|$ at 65°S demonstrating that the strongest ETCs transport the least moisture onto the Antarctic continent.

5. Cyclone Composites

Cyclone composites of MMF, TCWV and MSLP are now considered. Firstly this enables us to determine how the spatial pattern of the MMF, TCWV and MSLP relative to the ETC center depend on genesis latitude, maximum intensity and poleward propagation speed. Secondly, by considering TCWV and MSLP in addition to MMF it is possible to estimate the relative importance of moisture availability and system relative winds in contributing to MMF. Finally, by considering composites at different stages of ETC development, it is possible to ascertain if the relationships between genesis latitude, maximum intensity, propagation speed and MMF identified in section 4 apply throughout the ETC life cycle. However, it should be noted that in contrast to the results presented in section 5, where the moisture flux at certain latitudes was considered, the cyclone composites presented here contain cyclones at the same time relative to their maximum intensity and hence the cyclones are located at a range of latitudes.

The ETC composites 24 hours before the time of maximum intensity (Figures 7 and 8) show that for all bins the MMF has a maximum downstream of the ETC center in the warm sector where the TCWV has its largest values. However, the MMF, TCWV and MSLP spatial patterns vary significantly between the different bins in both JJA and DJF.

©2018 American Geophysical Union. All rights reserved.

Accepted Article

ETCs which have their genesis latitudes equatorward of 35°S have weak horizontal pressure gradients and symmetrical MSLP patterns, yet large values of poleward MMF in JJA (Figure 7c) and even more so in DJF (Figure 8c). In JJA, the TCWV values downstream and equatorward of the ETC center exceed 30 kg m^{-2}, and 50 kg m^{-2} in DJF, demonstrating that the large poleward MMF is primarily due to large values of local moisture rather than strong meridional system relative winds. In both JJA and DJF, ETCs with genesis latitudes in the mid-latitudes (Figures 7b and 8b) have stronger MSLP gradients and thus stronger system relative meridional winds than ETCs with genesis regions closer to the equator (composites of 900-hPa wind speed are shown in Figures S2 and S3 of the supporting material). However, the MMF is still reduced as the TCWV is much lower which indicates that the availability of moisture still dominates the MMF pattern. For ETCs with genesis latitudes close to the poles, the MSLP pattern indicates a more zonal flow which combined with the very low values of TCWV in these regions leads to weak MMF (Figures 7a and 8a).

In JJA and DJF, the ETC composites with the strongest maximum vorticity (Figures 7f and 8f) have strong MSLP gradients downstream of the ETC center co-located with high values of TCWV. In comparison to the composite ETCs with the most equatorward genesis regions (Figures 7c and 8c) or the fastest propagation speeds (Figures 7i and 8i), the composite ETCs with the strongest maximum intensity have stronger MSLP gradients and more meridional flow upstream of the ETC center. This results in a considerable amount of equatorward moisture transport which decreases the net poleward MMF. In both JJA and DJF, the average intensity composite ETCs (Figures 7e and 8e) and the weakest ETCs (Figures 7d and 8d) have very similar TCWV values. Thus, the weaker

©2018 American Geophysical Union. All rights reserved.

Accepted Article

MMF in the weakest ETC composite is due to weaker MSLP gradients and weaker system relative winds (see Figures S1 and S2).

ETCs which move the fastest (Figures 7i and 8i) have a different MSLP and TCWV structure compare to the other "top" bins (Figures 7a,d and 8a,d). In both JJA and DJF, the fastest moving ETC composites do not have a closed low associated with them. Instead, these ETCs resemble frontal waves and have large values of poleward MMF over a meridionally extensive but zonally narrow area. Furthermore, the ETCs with the fastest poleward propagation speed do not have any equatorward MMF on the upstream side of the cyclone. In contrast, the slowest moving ETCs have closed low pressure centers and broader areas of high TCWV. However, the large values of MMF associated with the fastest moving ETCs are likely enhanced by the large-scale, low-frequency flow that these ETCs may be embedded in. *Binder et al.* [2017] analyzed an ETC which lead to extreme poleward heat transport and concluded one reason for this was the superposition of ETCs (synoptic-scale variability) and a stationary anticyclone (low-frequency variability). Similarly, in an idealized study *Tamarin and Kaspi* [2017] show that the poleward deflection of the ETCs can be affected by stationary waves and thus low-frequency variability likely affects the poleward propagation speed of ETCs. However, an in-depth analysis of the low-frequency flow contribution to the poleward movement of ETCs and their MMF is beyond the scope of the current study.

The composites are only shown 24 hours before the time of maximum intensity, however, the time dependence of the composite spatial mean TCWV and MMF are shown in Figure 9 for JJA and Figure 10 for DJF. For each bin and offset time (i.e. each composite), the

©2018 American Geophysical Union. All rights reserved.

Accepted Article

spatial mean TCWV and MMF, weighted by grid area, is calculated over the circular 11 (DJF) or 12 (JJA) degree radius cap centered on each composite.

In JJA and DJF, TCWV and MMF are largest for ETCs with genesis latitudes closest to the equator at all offset times. Statistically significant positive linear relationships between mean TCWV and genesis latitude and mean MMF and genesis latitude are present at all offset times (Table 4) demonstrating that the relationship found between genesis latitude and MMF in section 4 is valid throughout the ETC life cycle. For all genesis latitude bins, TCWV and MMF decrease in a similar manner with increasing offset time which strongly indicates that the relationship between genesis latitude and MMF is primarily driven by moisture availability. However, TCWV has a maximum value at -48 hrs whereas MMF peaks at -24 hrs which suggests that in the developing part of the life cycle, the system relative winds or system speed can play a secondary role in determining the MMF.

In comparison to the genesis latitude bins, the variation of mean TCWV with maximum vorticity is small at all offset times in both JJA (Figure 9c) and DJF (Figure 10c). TCWV decreases with increasing offset time for all bins but the rate of decrease is greater for stronger ETCs: at -48 and -24 hrs, TCWV is higher in the strongest ETCs but at later offset times, TCWV is higher for weaker ETCs. Consequently, in JJA, there is no statistically significant relationship between TCWV and maximum vorticity at -48, -24 or 0 hours but at both 24 and 48 hours, there is a statistically significant negative correlation (Table 4). Similarly in DJF, a significant positive linear relationship exists at -48 hours and statistically significant negative relationships occur at 0, 24 and 48 hours. Despite the lack of significant positive relationship between TCWV and maximum vorticity, the mean MMF does increase with maximum vorticity in the early stages of the ETC life cycle.

©2018 American Geophysical Union. All rights reserved.

Accepted Article

Positive statistically significant linear relationships exists between MMF and maximum vorticity -48, -24 and +48 hours in JJA and at -48, -24 and 0 hours in DJF. Thus, it can be concluded that the positive correlation between MMF and maximum vorticity must be primarily due to variations in the meridional wind field. Given that the positive linear regression between maximum vorticity and MMF is only present during the intensification part of the ETC life cycle it is likely that the masking method, which includes all stages of the ETC simultaneously, will underestimate the correlation between maximum intensity and MMF.

The mean TCWV of the ETC composites with different speeds also decreases with increasing offset time for both JJA and DJF (figures 9e, 10e). The fastest moving ETCs experience a more rapid decrease in TCWV than the slowest moving ETCs as the fastest ETCs rapidly travel to higher latitudes where climatologically the TCWV is lower. This results in negative statistically significant linear relationships between speed and TCWV at 0, +24 and +48 hours in both DJF and JJA (Table 4). At -48 and -24 hrs, there are weak positive or negative correlations between TCWV and speed in JJA, but despite this MMF increases greatly with increasing speed and strong significant positive correlations evident between MMF and ETC speed in both DJF and JJA. This demonstrates that before the ETCs reach their maximum intensity the correlation between MMF and speed is not driven by moisture availability and consequently must be due to either system relative winds (as suggested by Figures 7i and 8i) or the system propagation speed (which may be influenced by low-frequency variability and stationary waves) or a combination of both. MMF peaks at -24 hours for all speed bins in both JJA and DJF and decreases after this. As was the case with TCWV, the MMF decreases faster with offset time for

©2018 American Geophysical Union. All rights reserved.

Accepted Article

the fastest moving ETCs than for the slowest moving ETCs (figures 9f, 10f). After the time of maximum intensity negative correlations exist between speed and both TCWV and MMF indicating that the correlation between MMF and speed is driven by moisture availability.

5. Discussion and Conclusions

We investigate meridional moisture transport by synoptic-scale, extra-tropical cyclones in the Southern Hemisphere in all seasons but with more in depth analysis performed for summer (DJF) and winter (JJA). We identify and track Southern Hemisphere extra-tropical cyclones (ETCs) in ERA-Interim reanalysis data and calculate the vertically integrated meridional moisture flux (MMF) associated with ETCs.

We determine which ETC characteristics exert the strongest control on the amount of moisture transported polewards per cyclone. In SH winter, at 50°S, the ETC genesis latitude is most important in determining the poleward moisture flux, closely followed by the ETC poleward propagation speed whereas ETC maximum vorticity only exerts a weak control on the MMF. Near the Antarctic coastline, at 65°S, the most influential ETC characteristic is the ETC poleward propagation speed and again ETC maximum relative vorticity is found to be the least influential ETC characteristic. These results were not sensitive to the choice of ETC radius. In SH summer very similar results are found at 50°S as in winter and at 65°S ETC poleward propagation speed remains the most dominant ETC characteristic influencing the MMF per ETC. However, at 65° in SH summer, there is a statistically significant negative correlation between ETC maximum vorticity and MMF per ETC and no longer a significant relationship between genesis latitude and MMF per ETC.

©2018 American Geophysical Union. All rights reserved.

Accepted Article

We thus conclude that ETC poleward propagation speed has the strongest influence on ETC MMF, particularly at high latitudes, and that ETCs which travel quickly from low to high-latitudes are responsible for considerably more MMF to Antarctica than those which travel poleward slowly. This is likely because the moisture moves with the ETC as it travels polewards and is subject to less dilution and cycling. However, the poleward MMF of the fastest moving ETCs may be enhanced by transport by the low frequency background flow in which the ETCs is embedded within. This result suggests that if ETC tracks become more meridional in the future and hence if ETCs move poleward faster then the MMF due to ETCs would increase. *Tamarin-Brodsky and Kaspi* [2017] applied TRACK to CMIP5 models and showed that there is an increase in the latitudinal displacement of storms under global warming in all storm track regions (their Figure 3). Furthermore, *Kotila et al.* [2013] showed that the track orientation of ETCs near the Antarctic coastline become more meridional when the Southern Annular Mode (SAM) is positive and *Marshall* [2003] showed the SAM has exhibited a positive trend in recent years. Combined with our results, which indicate that cyclones with more meridional tracks transport more moisture, these earlier results could imply that in the future, poleward moisture transport, and in particular moisture transport to Antarctic may increase.

Our results also show that in the mid-latitudes genesis latitude exerts a strong control on $\mathrm{MMF_{ETC}}$ which means that if ETC genesis regions move polewards, then the $\mathrm{MMF_{ETC}}$ would decrease. However, in DJF the correlation between genesis latitude and ETC MMF decreases towards the pole, indicating that the MMF associated with a ETC near the Antarctic coastline is only weakly influenced by the environment in which it forms. This in turn suggests that by the time the ETC reaches Antarctica, the original sub-tropical

©2018 American Geophysical Union. All rights reserved.

Accepted Article

moist air is almost completely diluted by moisture evaporated from higher latitudes, a consequence of continuous cycling of moisture within the ETC itself.

Composites of ETCs elucidate the reason that propagation speed exerts the dominant control on ETC MMF. First, fast moving ETCs resembles a frontal wave whereas the most intense ETCs and the ETCs with the lowest latitude genesis region both have closed low pressure centers. Second, the most intense ETCs and the ETCs originating at the lowest latitudes exhibit a MMF dipole with poleward MMF downstream, and equatorward MMF upstream, of their vorticity center whereas the fastest moving ETCs only exhibit poleward MMF and thus greater net MMF.

The time evolution of the correlations between ETC characteristics and the TCWV and MMF averaged over the ETC composites clarify the physical reasons for the relationships identified between ETC MMF and ETC characteristics. The correlation between genesis latitude and both TCWV and poleward MMF is strong throughout the entire ETC life cycle demonstrating that this relationship is driven by moisture availability. Thus, for an average strength ETC with average propagation velocity, local moisture availability dominates its MMF at all stages. No positive correlation between maximum vorticity and TCWV is found at any point of the ETC life cycle which is consistent with *Rudeva and Gulev* [2011] who found that the absolute value of precipitable water (PW) in the warm sector of their composite cyclones did not vary with cyclone intensity (their Figure 5b). Despite the lack of dependence of TCWV on ETC intensity, there is a positive correlation between maximum vorticity and MMF during the intensification stage (the MMF approximately doubles from weakest to strongest ETCs) which is driven by the system relative winds. The correlation between ETC poleward propagation speed and

©2018 American Geophysical Union. All rights reserved.

Accepted Article

TCWV changes sign during the ETC life cycle in JJA and becomes more negative in DJF as TCWV decreases more rapidly for the fastest moving ETCs. Similar results were reported by *Rudeva and Gulev* [2011] who also created ETC composites for different lysis regions and show that cyclones which moved the farthest polewards see the largest decrease in PW whereas those with the most zonal tracks have the smallest decrease in PW. During the developing stages the net poleward MMF approximately triples from slowest to fastest ETCs with increasing ETC speed whereas TCWV only increases by about 25% indicating that moisture availability does not drive the very strong correlation identified between ETC speed and MMF.

Climate models do not agree on how SH ETCs or Antarctic precipitation will respond to climate change [*Bengtsson et al.*, 2006]. In general they predict an increase in Antarctic precipitation [*Trenberth et al.*, 2003; *Frieler et al.*, 2015] but large spatial and seasonal variations exist in the predicted precipitation changes [*Bracegirdle et al.*, 2008]. Some models predict a reduction in the number of cyclones but with an increase in the number of intense cyclones [*Geng and Sugi*, 2003; *Lambert and Fyfe*, 2006]. There is some observational evidence to support this [*Pezza and Ambrizzi*, 2003]. The main result of this study — that ETC propagation speed exerts the strongest control on how much moisture a given extra tropical cyclone can transport polewards — suggest that in addition to future changes in ETC number and intensity, changes in ETC track orientation should be investigated. However, as current climate models have large biases in the location and strength of the SH storm track [e.g. *Barnes and Polvani*, 2013] accurately quantifying how ETC track orientation, and hence the meridional moisture flux, is likely to change in the future, will be challenging.

©2018 American Geophysical Union. All rights reserved.

Accepted Article

One aspect which was not considered in the current study is the potential role low-frequency variability can play in influencing moisture transport by ETCs. The partitioning of the synoptic and low-frequency components will form the subject of future work and will allow a link between weather diagnostics and climate variables to be made.

Acknowledgments. The ERA-Interim data was obtained freely from `http://apps.ecmwf.int/datasets/`. Information on how to obtain the cyclone identification and tracking algorithm can be found from `http://www.nerc-essc.ac.uk/~kih/TRACK/Track.html`. The cyclone tracks obtained from TRACK and used in this study are available from Zenodo data repository at http://doi.org/10.5281/zenodo.2559459. We thank Kevin Hodges for providing his ETC tracking code, Matt Hawcroft for providing his ETC mask code. We acknowledge ECMWF for making the ERA-Interim reanalysis data available and CSC – IT Center for Science Ltd. for the allocation of computational resources. VAS is funded by the Academy of Finland (project no. 307331). The Väisälä Foundation is acknowledged for funding HFD trips to Helsinki. We also thank 2 anonymous reviewers for their comments which helped improve this paper.

References

Arnau, S., E. Schlosser, E. Isaksson, and D. Divine (2015), Climatic signals from 76 shallow firn cores in Dronning Maud Land, East Antarctica, *The Cryosphere*, *9*(3), 925–944.

Barnes, E. A., and L. Polvani (2013), Response of the midlatitude jets, and of their variability, to increased greenhouse gases in the CMIP5 models, *J. Climate*, *26*(18), 7117–7135.

©2018 American Geophysical Union. All rights reserved.

Accepted Article

Bengtsson, L., K. I. Hodges, and E. Roeckner (2006), Storm tracks and climate change, *J. Climate*, *19*(15), 3518–3543.

Binder, H., M. Boettcher, C. M. Grams, H. Joos, S. Pfahl, and H. Wernli (2017), Exceptional air mass transport and dynamical drivers of an extreme wintertime arctic warm event, *Geophys. Res. Lett.*, *44*(23).

Bjerknes, J., and H. Solberg (1922), Life cycle of cyclones and the polar front theory of atmospheric circulation, *Geofys. Publ.*, *3*(1), 1–38.

Bracegirdle, T. J., W. M. Connolley, and J. Turner (2008), Antarctic climate change over the twenty first century, *J. Geophys. Res.*, *113*, doi:10.1029/2007JD008933, D03103.

Bromwich, D. H. (1988), Snowfall in high southern latitudes, *Reviews of Geophysics*, *26*(1), 149–168.

Bromwich, D. H. (1990), Estimates of Antarctic precipitation, *Nature*, *343*(6259), 627–629.

Carlson, T. N. (1980), Airflow through mid-latitude cyclones and the comma cloud pattern, *Mon. Wea. Rev.*, *108*, 1498–1509.

Catto, J. L., L. C. Shaffrey, and K. I. Hodges (2010), Can climate models capture the structure of extratropical cyclones?, *Journal of Climate*, *23*(7), 1621–1635.

Dacre, H. F., M. K. Hawcroft, M. A. Stringer, and K. I. Hodges (2012), An extratropical cyclone atlas: A tool for illustrating cyclone structure and evolution characteristics, *Bull. Amer. Meteor. Soc.*, *93*(10), 1497–1502.

Davis, C. H., Y. Li, J. R. McConnell, M. M. Frey, and E. Hanna (2005), Snowfall-driven growth in East Antarctic ice sheet mitigates recent sea-level rise, *Science*, *308*(5730), 1898–1901.

©2018 American Geophysical Union. All rights reserved.

Accepted Article

Delaygue, G., V. Masson, J. Jouzel, R. D. Koster, and R. J. Healy (2000), The origin of Antarctic precipitation: a modelling approach, *Tellus B*, *52*(1).

Field, P. R., and R. Wood (2007), Precipitation and cloud structure in midlatitude cyclones, *J. Climate*, *20*(2), 233–254.

Frieler, K., P. U. Clark, F. He, C. Buizert, R. Reese, S. R. Ligtenberg, M. R. van den Broeke, R. Winkelmann, and A. Levermann (2015), Consistent evidence of increasing Antarctic accumulation with warming, *Nature Climate Change*.

Fyfe, J. C. (2003), Extratropical Southern Hemisphere cyclones: harbingers of climate change?, *J. Climate*, *16*, 2802–2805.

Geng, Q., and M. Sugi (2003), Possible change of extratropical cyclone activity due to enhanced greenhouse gases and sulfate aerosols-study with a high-resolution AGCM, *J. Climate*, *16*(13), 2262–2274.

Gorodetskaya, I. V., M. Tsukernik, K. Claes, M. F. Ralph, W. D. Neff, and N. P. M. Van Lipzig (2014), The role of atmospheric rivers in anomalous snow accumulation in East Antarctica, *Geophys. Res. Lett.*, *41*, 6199–6206, doi:10.1002/2014GL060881.

Govekar, P. D., C. Jakob, M. J. Reeder, and J. Haynes (2011), The three-dimensional distribution of clouds around southern hemisphere extratropical cyclones, *Geophys. Res. Lett.*, *38*(21).

Hawcroft, M. K., L. C. Shaffrey, K. I. Hodges, and H. F. Dacre (2012), How much Northern Hemisphere precipitation is associated with extratropical cyclones?, *Geophys. Res. Lett.*, *39*(24).

Hodges, K. I. (1994), A general method for tracking analysis and its application to meteorological data, *Mon. Wea. Rev.*, *122*, 2573–2586.

©2018 American Geophysical Union. All rights reserved.

Accepted Article

Hodges, K. I. (1995), Feature tracking on the unit-sphere, *Mon. Wea. Rev.*, *123*(12), 3458–3465.

Hoskins, B. J., and K. I. Hodges (2005), A new perspective on Southern Hemisphere storm tracks, *J. Climate*, *18*(20), 4108–4129.

Jung, T., M. J. Miller, T. N. Palmer, P. Towers, N. Wedi, D. Achuthavarier, J. M. Adams, E. L. Altshuler, B. A. Cash, J. L. Kinter Iii, et al. (2012), High-resolution global climate simulations with the ECMWF model in Project Athena: Experimental design, model climate, and seasonal forecast skill, *J. Climate*, *25*(9), 3155–3172.

Krinner, G., C. Genthon, Z.-X. Li, and P. Le Van (1997), Studies of the Antarctic climate with a stretched-grid general circulation model, *J. Geophys. Res.*, *102*(D12), 13,731–13,745.

Lambert, S. J., and J. C. Fyfe (2006), Changes in winter cyclone frequencies and strengths simulated in enhanced greenhouse warming experiments: results from the models participating in the IPCC diagnostic exercise, *Climate Dynamics*, *26*(7-8), 713–728.

Marshall, G. (2003), Trends in the Southern Annular Mode from observations and reanalyses, *J. Climate*, *16*, 4134–4143.

[redacted] D., J. Turner, and R. Mulvaney (1999), Atmospheric signals and characteristics of accumulation in Dronning Maud Land, Antarctica, *J. Geophys. Res.*, *104*, 19,191–19,211.

[redacted]r, A., T. Phillips, S. Webster, A. Elvidge, M. Weeks, S. Hosking, and J. Turner (2014), The Met Office Unified Model high-resolution simulations of a strong wind event in Antarctica, *Q. J. R. Meteorol. Soc.*, *140*, 2287–2297.

©2018 American Geophysical Union. All rights reserved.

Accepted Article

Papritz, L., S. Pfahl, I. Rudeva, I. Simmonds, H. Sodemann, and H. Wernli (2014), The role of extratropical cyclones and fronts for Southern Ocean freshwater fluxes, *J. Climate*, *27*(16), 6205–6224.

Parish, T. R., and D. H. Bromwich (1998), A case study of Antarctic katabatic wind interaction with large-scale forcing, *Mon. Wea. Rev.*, *126*, 119–209.

Pezza, A. B., and T. Ambrizzi (2003), Variability of Southern Hemisphere cyclone and anticyclone behavior: Further analysis, *J. Climate*, *16*(7), 1075–1083.

Sodemann, S., E. Madonna, M. Boettcher, H. Joos, and H. Wernli (2014), Warm conveyor belts in the era-interim dataset (1979–2010). part ii: Moisture origin and relevance for precipitation, *J. Climate*, *27*(1), 27–40.

Roberts, J., C. Plummer, T. Vance, T. van Ommen, A. Moy, S. Poynter, A. Treverrow, M. Curran, and S. George (2015), A 2000-year annual record of snow accumulation rates for Law Dome, East Antarctica, *Climate of the Past*, *11*(5), 697–707.

Rudeva, I., and S. K. Gulev (2007), Climatology of cyclone size characteristics and their changes during the cyclone life cycle, *Mon. Wea. Rev.*, *135*(7), 2568–2587.

Rudeva, I., and S. K. Gulev (2011), Composite analysis of North Atlantic extratropical cyclones in NCEP-NCAR reanalysis data, *Mon. Wea. Rev.*, *139*(5), 1419–1446.

Schoen, N., A. Zammit-Mangion, J. C. Rougier, T. Flament, F. Rémy, S. Luthcke, and J. L. Bamber (2015), Simultaneous solution for mass trends on the West Antarctic Ice Sheet, *The Cryosphere*, *9*(2), 805–819.

Seo, K.-W., C. R. Wilson, T. Scambos, B.-M. Kim, D. E. Waliser, B. Tian, B.-H. Kim, and J. Eom (2015), Surface mass balance contributions to acceleration of Antarctic ice mass loss during 2003–2013, *J. Geophys. Res.*

©2018 American Geophysical Union. All rights reserved.

Accepted Article

Shapiro, M. A., and D. Keyser (1990), *Extratropical Cyclones: The Erik Palmén Memorial Volume*, chap. Fronts, jet streams and the tropopause, pp. 167–191, Amer. Meteor. Soc.

Sinclair, V. A., and H. F. Dacre (2019), Southern Hemisphere cyclones tracks 1979-2013, doi:10.5281/zenodo.2559459.

Sodemann, H., and A. Stohl (2009), Asymmetries in the moisture origin of Antarctic precipitation, *Geophys. Res. Lett.*, *36*(22).

Tamarin, T., and Y. Kaspi (2017), Mechanisms controlling the downstream poleward deflection of midlatitude storm tracks, *J. Atmos. Sci.*, *74*(2), 553–572.

Tamarin-Brodsky, T., and Y. Kaspi (2017), Enhanced poleward propagation of storms under climate change, *Nature Geoscience*, *10*(12), 908.

Tietäväinen, H., and T. Vihma (2008), Atmospheric moisture budget over Antarctica and the Southern Ocean based on the ERA-40 reanalysis, *Int. J. Climatol.*, *28*, 1977–1995.

Trenberth, K. E., A. Dai, R. M. Rasmussen, and D. B. Parsons (2003), The changing character of precipitation, *Bull. Amer. Meteor. Soc.*, *84*(9), 1205–1217.

Tsukernik, M., and A. H. Lynch (2013), Atmospheric meridional moisture flux over the Southern Ocean: a story of the Amundsen Sea, *J. Climate*, *26*, 8055–8064.

[redacted] P., T. Vihma, and M. Tsukernik (2013), Close interactions between the antarctic cyclone budget and large-scale atmospheric circulation, *Geophys. Res. Lett.*, *40*(12), 3237–3241.

Usumi, N., H. Kim, S. Kanae, and T. Oki (2016), Relative contributions of weather systems to mean and extreme global precipitation, *Journal of Geophysical Research: Atmospheres*, *122*(1), 152–167, doi:10.1002/2016JD025222.

©2018 American Geophysical Union. All rights reserved.

Accepted Article

Wang, X. L., and F. W. Swail, V. R. amd Zwiers (2006), Climatology and changes of extratropical cyclone activity: Comparison of ERA-40 with NCEP–NCAR reanalysis for 19582001, *J. Climate*, *19*, 3145–3166.

Williams, L. N., S. Lee, and S.-W. Son (2007), Dynamics of the Southern Hemisphere Spiral Jet, *J. Atmos. Sci.*, *64*, 548563.

Zappa, G., L. C. Shaffrey, and K. I. Hodges (2013), The ability of CMIP5 models to simulate North Atlantic extratropical cyclones, *J. Climate*, *26*(15), 5379–5396.

Zappa, G., M. K. Hawcroft, L. Shaffrey, E. Black, and D. J. Brayshaw (2015), Extratropical cyclones and the projected decline of winter Mediterranean precipitation in the CMIP5 models, *Climate Dynamics*, *45*(7-8), 1727–1738.

Accepted Article

©2018 American Geophysical Union. All rights reserved.

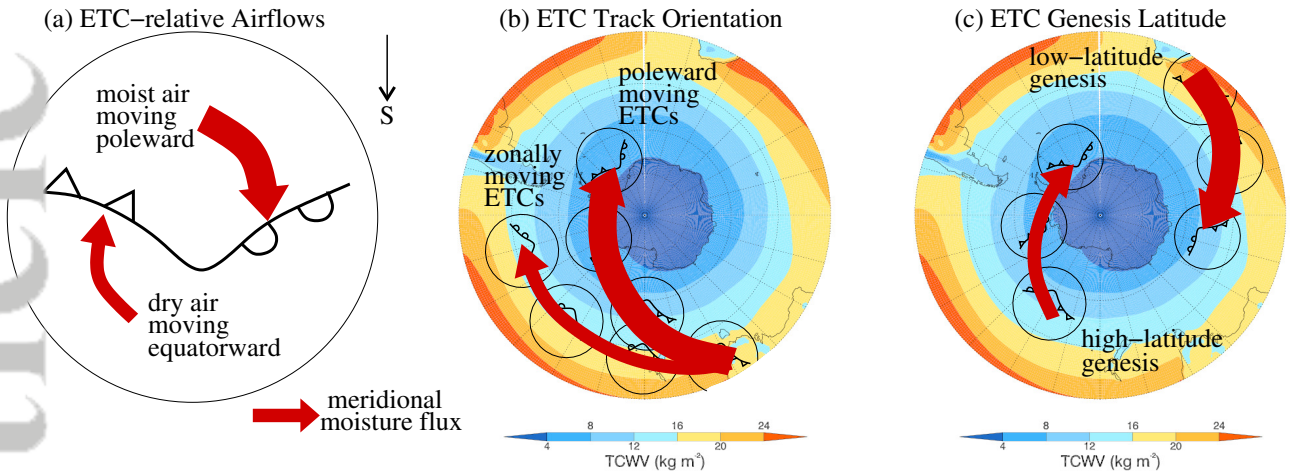


Figure 1. Schematic demonstrating the MMF associated with (a) ETC-relative airflows, (b) ETC track orientations and (c) ETC genesis latitudes. (b) and (c) overlaid on 1979-2014 annual mean total column water vapor (TCWV). The width of the arrows indicate the relative magnitude of the MMF.

Accepted Article

©2018 American Geophysical Union. All rights reserved.

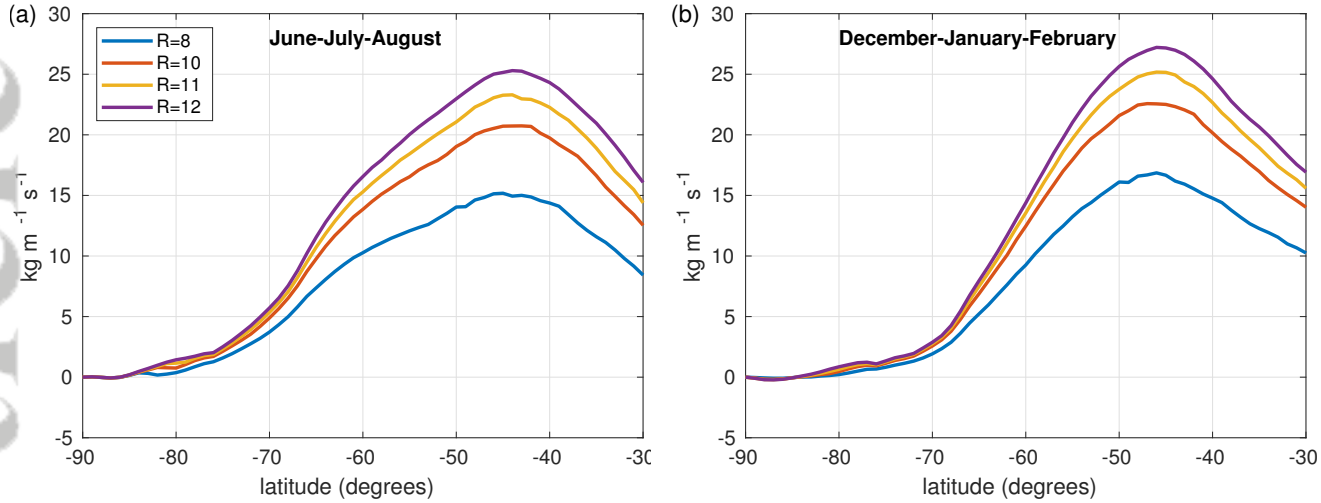


Figure 2. Sensitivity of the annual and zonal mean (calculated over 35 years of ERA-Interim data) net ETC-related meridional moisture flux due to the definition of the ETC radius for (a) JJA and (b) DJF. Blue lines show an ETC radius of 8 degrees, orange lines 10 degrees, yellow lines 11 degrees, and purple lines 12 degrees.

Table 1. Bins used to determine the effect of maximum vorticity, the genesis latitude and the poleward propagation velocity of ETCs on the ETC-related meridional moisture transport. The divisions between the bins were determined by first analyzing probability density functions (PDFs) of each predictor variable.

Bin	Max vorticity (s^{-1})	Genesis Latitude (°S)	Poleward Velocity (degrees per day)
1	1.0 – 5.0 $\times 10^{-5}$	> 67.5	0 – 2
2	5.0 – 6.5 $\times 10^{-5}$	62.5 – 67.5	2 – 4
3	6.5 – 8.0 $\times 10^{-5}$	55.0 - 62.5	4 – 6
4	8.0 – 9.5 $\times 10^{-5}$	45.0 - 55.0	6 – 8
5	9.5 – 10.5 $\times 10^{-5}$	35.0 – 45.0	8 – 10
6	>10.5 $\times 10^{-5}$	<35.0	>10

Accepted Article

©2018 American Geophysical Union. All rights reserved.

Accepted Article

Table 2. Regression coefficients for simple linear regression conducted between the standardized predictors and the zonally averaged ETC-related MMF per ETC mask, $\overline{|MMF_{ETC}|}$ at different latitudes in JJA and DJF. Predictors are centered on their mean values and normalized by their standard deviation. Values in bold are statistically significant at the 99% level. Italic values are statistically significant at the 95% level.

latitude	genesis lat JJA	genesis lat DJF	vorticity JJA	vorticity DJF	speed JJA	speed DJF
40°S	**34.72**	**36.03**	0.92	*14.26*	**37.79**	**46.02**
45°S	**35.43**	**43.84**	0.44	*9.56*	**34.52**	**45.22**
50°S	**30.54**	**39.80**	0.96	*4.31*	**27.54**	**37.99**
55°S	**24.29**	*26.61*	**2.88**	**1.84**	**19.12**	**27.34**
60°S	**14.40**	*10.35*	**3.02**	-0.11	**12.80**	**18.41**
65°S	**7.28**	2.65	**2.21**	-1.03	**7.86**	**10.96**
70°S	**2.97**	0.54	*1.28*	-0.33	**3.92**	**4.69**
75°S	**1.65**	0.54	*1.07*	0.74	**1.99**	*1.85*

Table 3. Regression coefficients for multiple linear regression conducted between the standardize predictors and the zonally averaged ETC-related MMF per ETC mask, $\overline{|MMF_{ETC}|}$ at different latitudes in JJA and DJF. Predictors are centered on their mean values and normalized by their standard deviation. Values in bold are statistically significant at the 99% level. Italic values are statistically significant at the 95% level.

Season	JJA		DJF	
Latitude	50°S	65°S	50°S	65°S
90-genesis lat	**1.89**	**1.00**	**2.99**	0.14
vorticity	**0.80**	-0.01	**3.50**	**-0.73**
speed	**5.83**	**2.46**	**5.69**	**2.59**
vorticity:speed	**-0.78**	-0.16	-0.34	-0.15
vorticity:90-genesis lat	**-0.75**	**-0.37**	**-0.88**	**-1.40**
speed:90-genesis lat	*-0.43*	4.4×10^{-3}	-0.67	*0.32*

©2018 American Geophysical Union. All rights reserved.

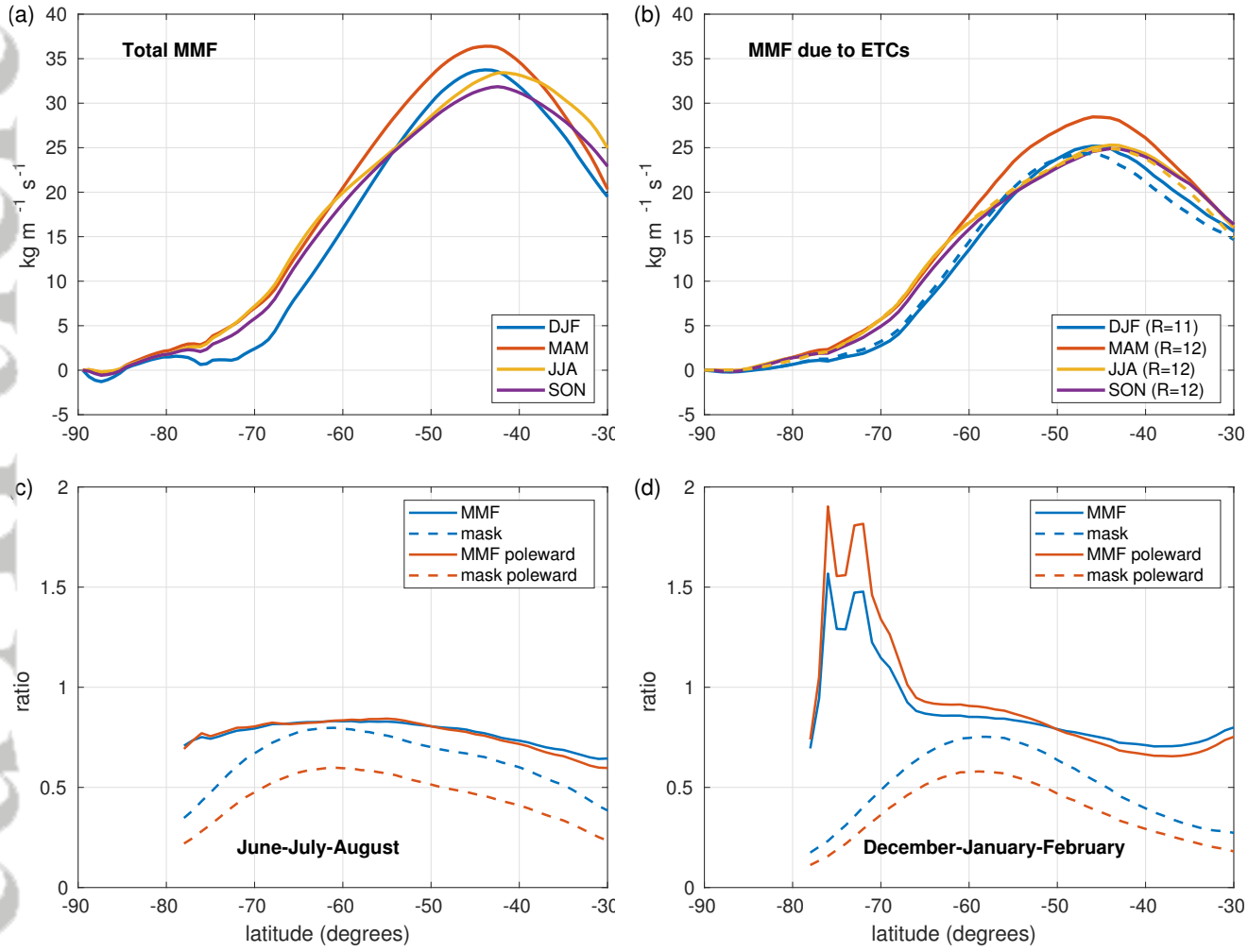


Figure 3. Zonally averaged (a) total meridional moisture flux, $\overline{MMF_{TOT}}$, and (b) ETC-related dional moisture flux, $\overline{MMF_{ETC}}$, assuming a radius of 12 degrees in all seasons except DJF where 11 degrees is used, for DJF (red), MAM (orange), JJA (yellow) and SON (purple). Solid lines in (b) show meridional moisture flux due to all ETCs, dashed lines show meridional moisture flux due to poleward moving ETCs. (c) and (d) shows the ratio of ETC MMF to total MMF (solid lines) and the zonal mean occurrence of ETC masks at each latitude (dashed lines) for JJA and DJF respectively. Blues lines show ratios when all ETCs are considered and orange lines show ratios when only poleward moving ETCs are considered.

©2018 American Geophysical Union. All rights reserved.

Accepted Article

Accepted Article

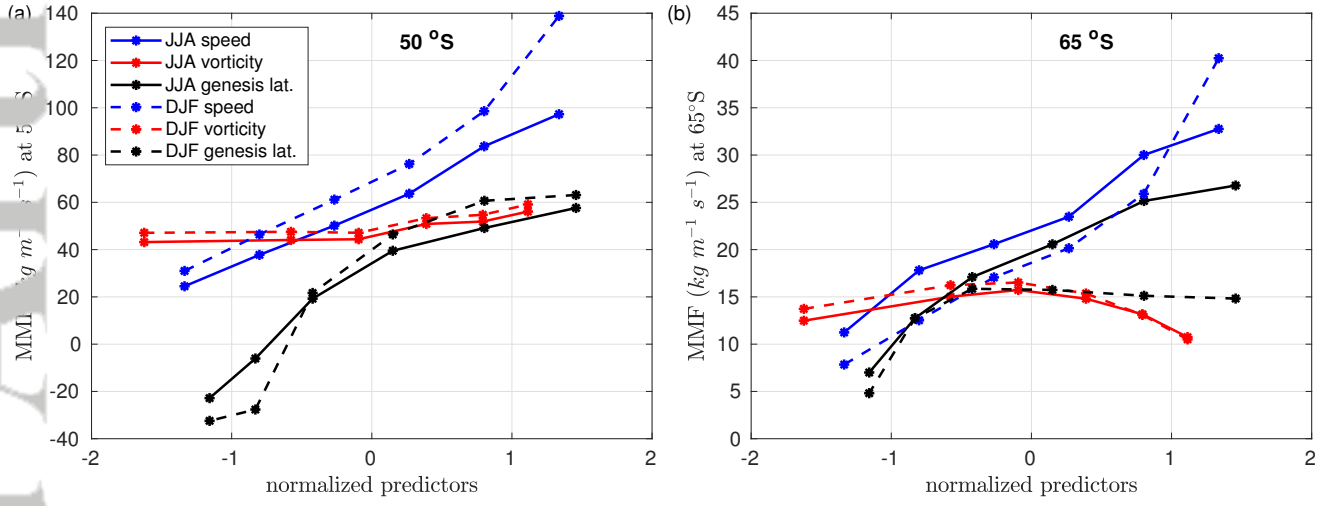


Figure 4. Relationship between ETC characteristics and zonally averaged ETC-related MMF for ETC mask, $\overline{|MMF_{ETC}|}$ at (a) 50°S and (b) 65°S for JJA (solid lines) and DJF (dashed lines). Predictor variables are centered on their mean and normalized by their standard deviation. The ETC characteristics are poleward propagation velocity (blue), maximum cyclonic vorticity (red), and genesis latitude (black). Genesis latitude is represented by 90 - genesis latitude (distance from south pole). Only poleward moving ETCs are included. Slope coefficients are shown in Table 1. Note the different y-axis between the two panels.

©2018 American Geophysical Union. All rights reserved.

Accepted Article

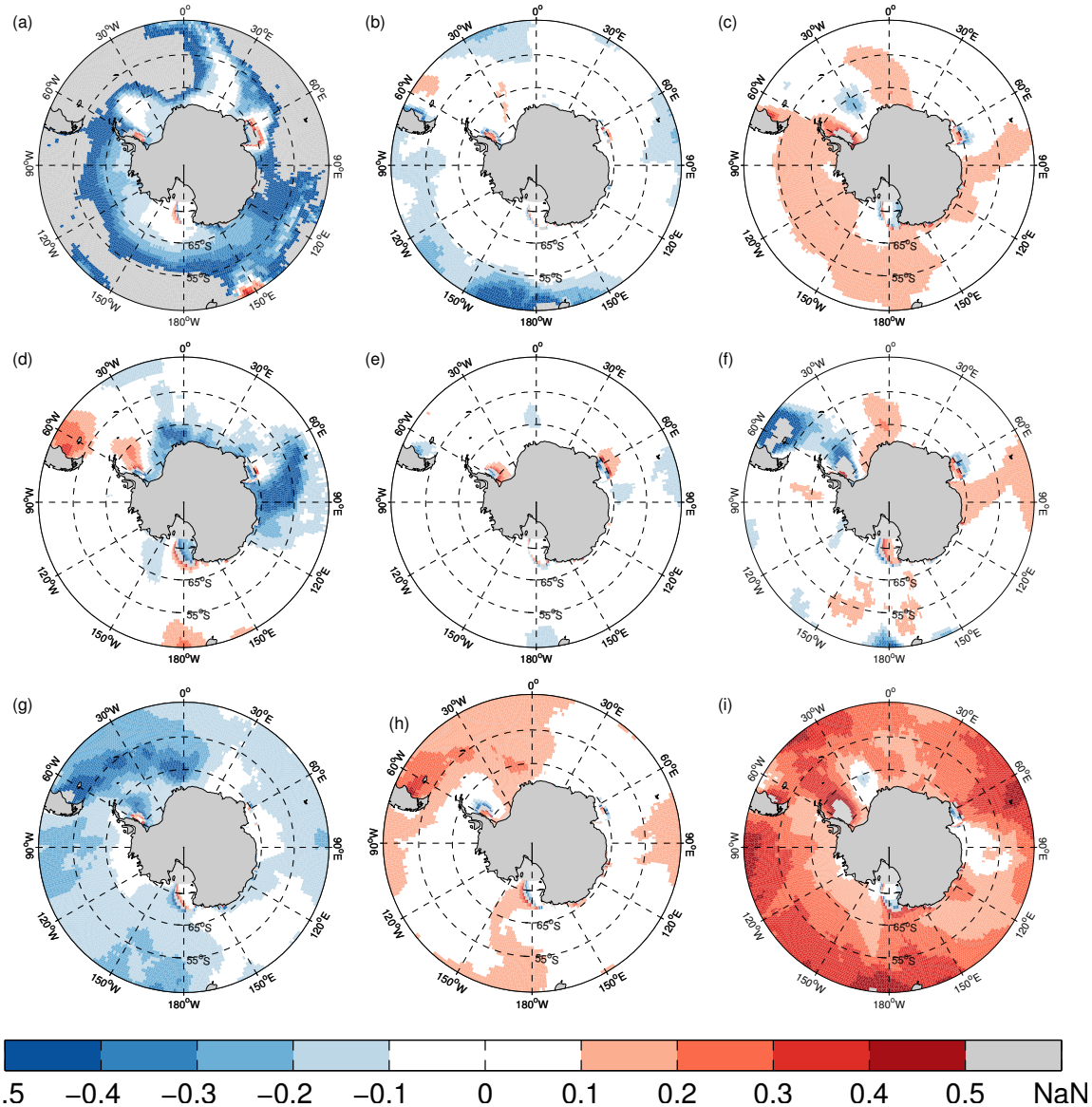


Figure 5. JJA: $\log_{10}$ of the ratio between MMF per ETC for a given bin, i, $|MMF_{ETC}|^i$, and the MMF per ETC for all ETCs, $|MMF_{ETC}|$. Top row: different genesis latitudes. (a) south of 62.5°S, (b) 45–62.5°S and (c) north of 45°S. Middle row: different maximum 850-hPa relative vorticity. (d) less than 6.5 $\times 10^{-5}$ s^{-1}, (e) 6.5 $\times 10^{-5}$–9.5 $\times 10^{-5}$ s^{-1}, (f) greater than 9.5 $\times 10^{-5}$ s^{-1}. Bottom row: different meridional speed. (g) less than 4 degrees latitude per day, (h) 4 – 8 degrees latitude per day, (i) greater than 8 degrees latitude per day. Only poleward moving ETCs are considered. Grey areas are where the ratio ($|MMF_{ETC}|^i$ / $|MMF_{ETC}|$) is negative or over Antarctica.

©2018 American Geophysical Union. All rights reserved.

Accepted Article

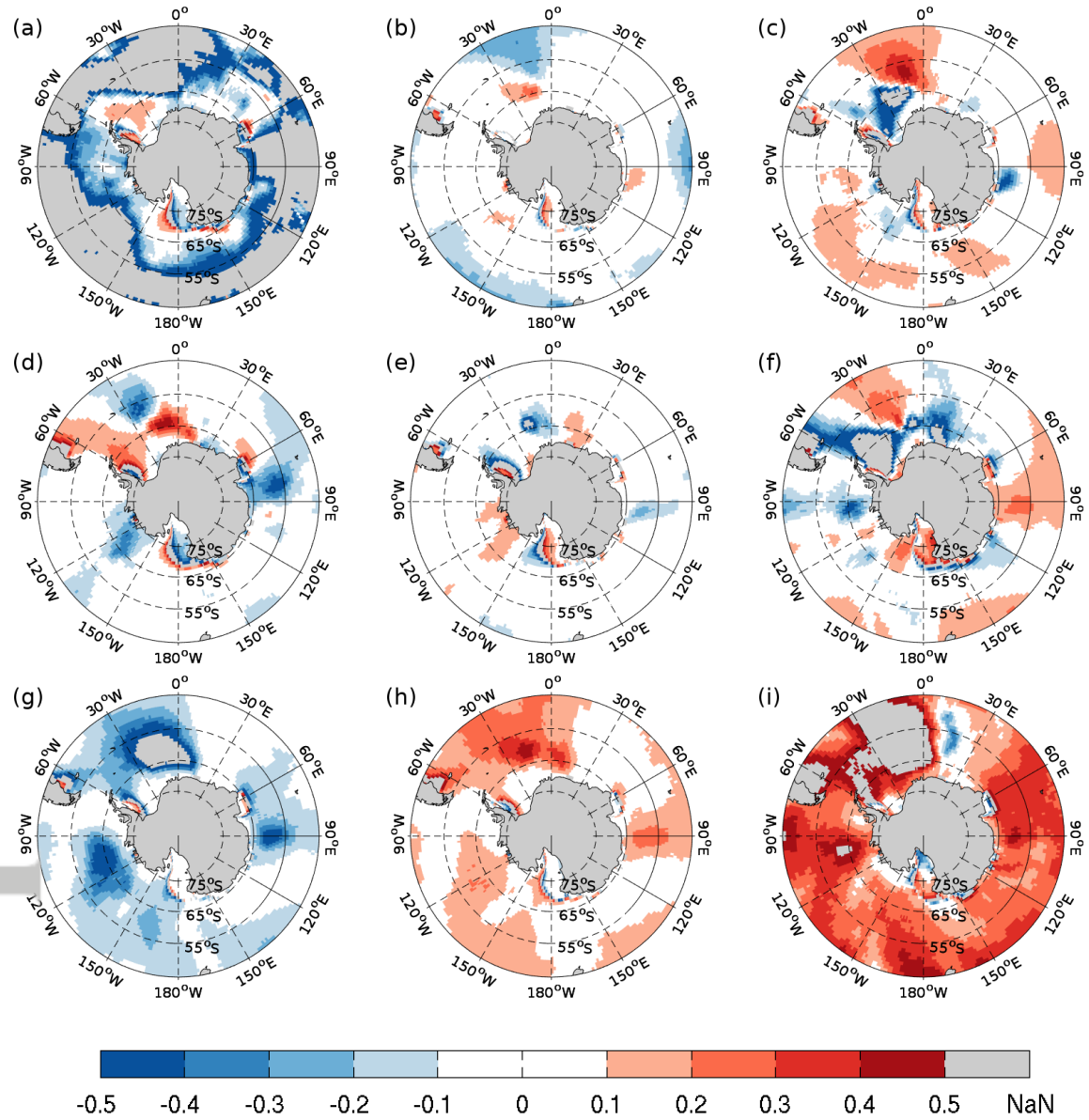


Figure 6. DJF: $\log_{10}$ of the ratio between MMF per ETC for a given bin, i, $|MMF_{ETC}|^i$, and the MMF per ETC for all ETCs, $|MMF_{ETC}|$. Top row: different genesis latitudes. (a) south of 62.5°S, (b) 45–62.5°S and (c) north of 45°S. Middle row: different maximum 850-hPa relative vorticity. (d) less than 6.5 $\times 10^{-5}$ s^{-1}, (e) 6.5 $\times 10^{-5}$–9.5 $\times 10^{-5}$ s^{-1}, (f) greater than 9.5 $\times 10^{-5}$ s^{-1}. Bottom row: different meridional speed. (g) less than 4 degrees latitude per day, (h) 4–8 degrees latitude per day, (i) greater than 8 degrees latitude per day. Only poleward moving

D R A F T February 8, 2019, 8:55am D R A F T

©2018 American Geophysical Union. All rights reserved.

Accepted Article

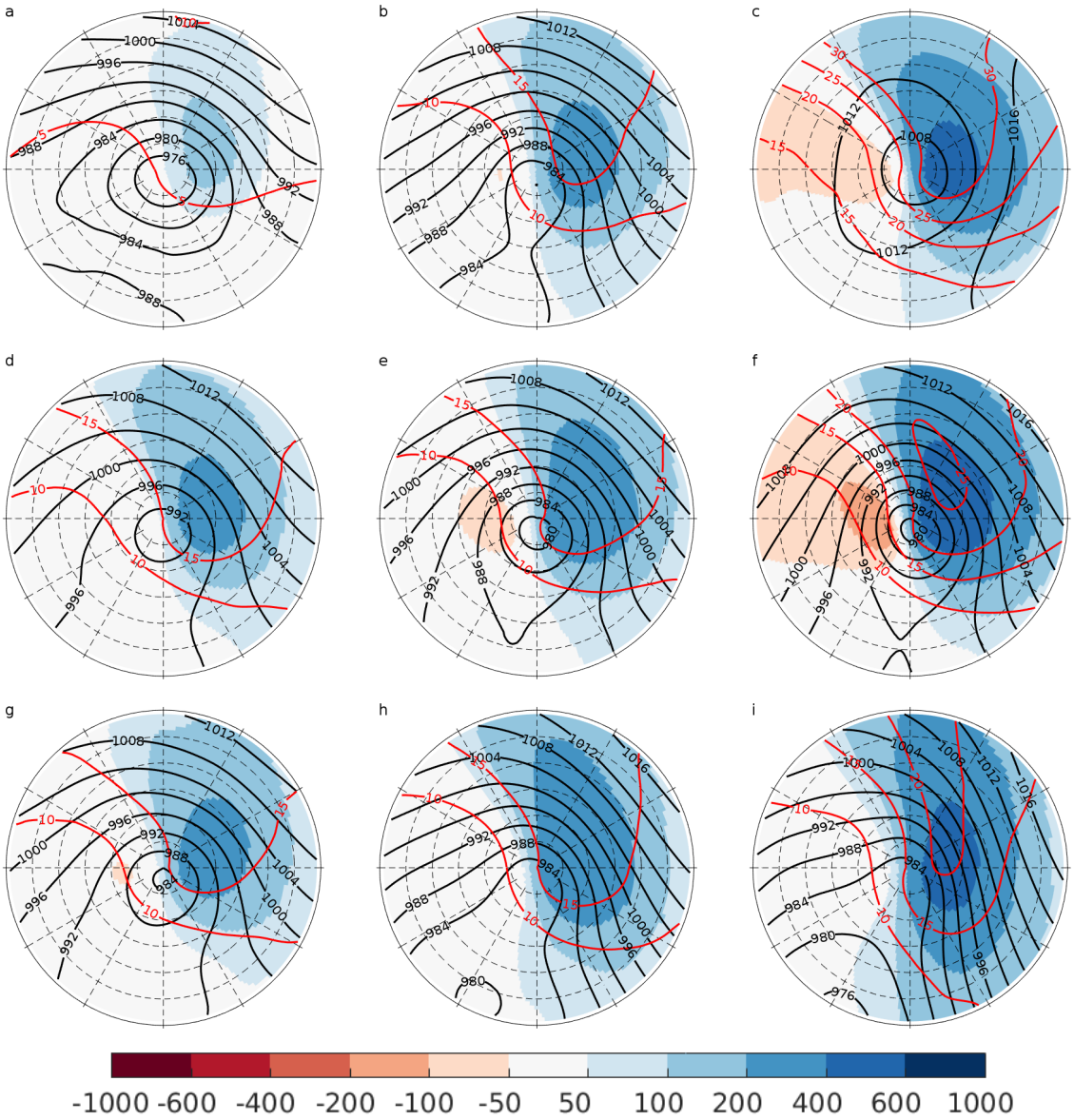


Figure 7. Composites of the meridional moisture flux (shading, kg $m^{-1}s^{-1}$), MSLP (black contours, hPa) and TCWV (red contours, kg m^{-2}) for ETCs occurring in JJA 24 hours before the time of maximum vorticity. Different genesis latitude bins (a-c), maximum vorticity bins (d-f) and speed bins (g-i). Left column shows bin 2, center column bin 4 and right column bin

©2018 American Geophysical Union. All rights reserved.

Accepted Article

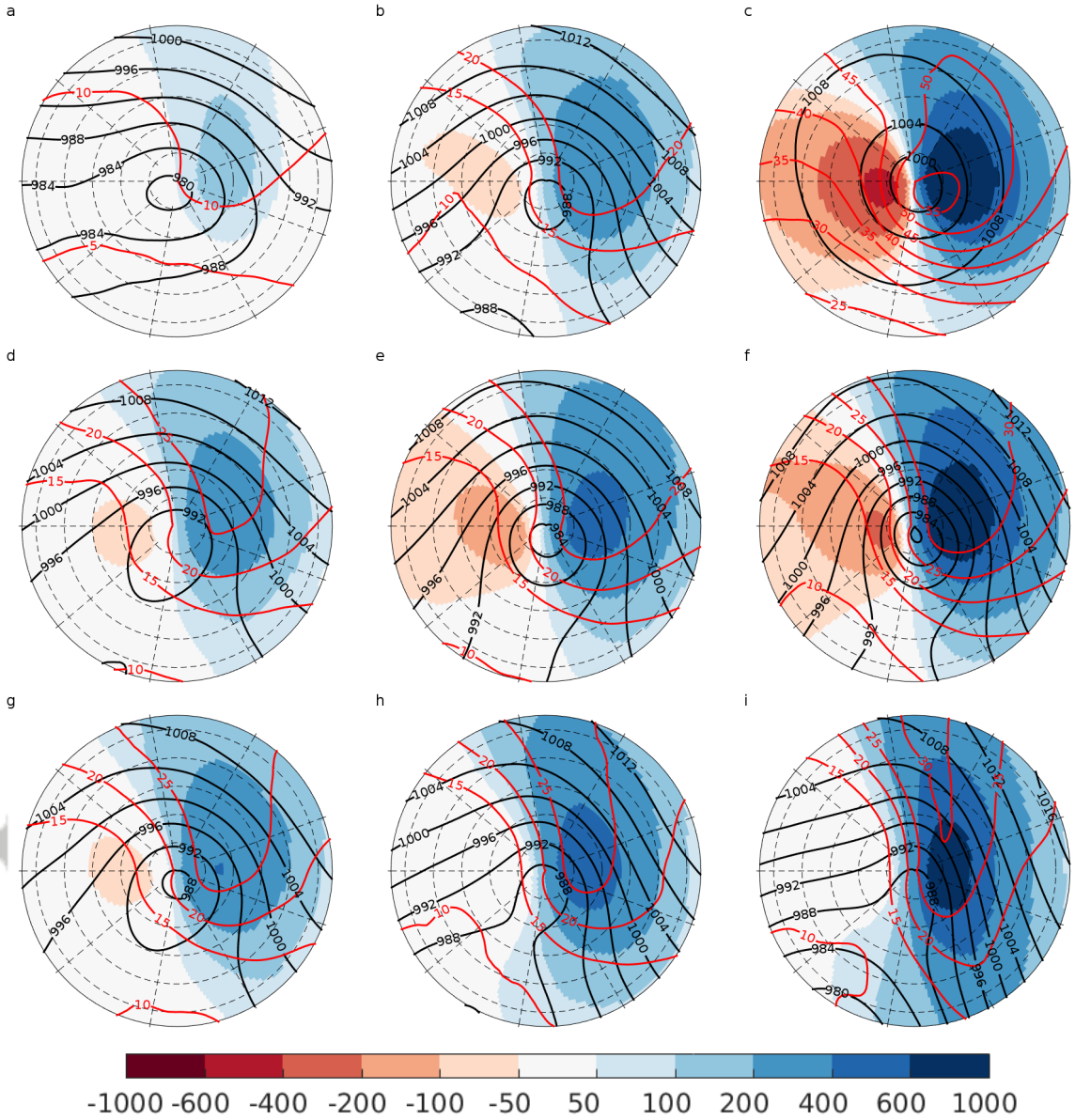


Figure 8. Same as Figure 7 except for DJF and with a radius of 11 degrees.

©2018 American Geophysical Union. All rights reserved.

Accepted Article

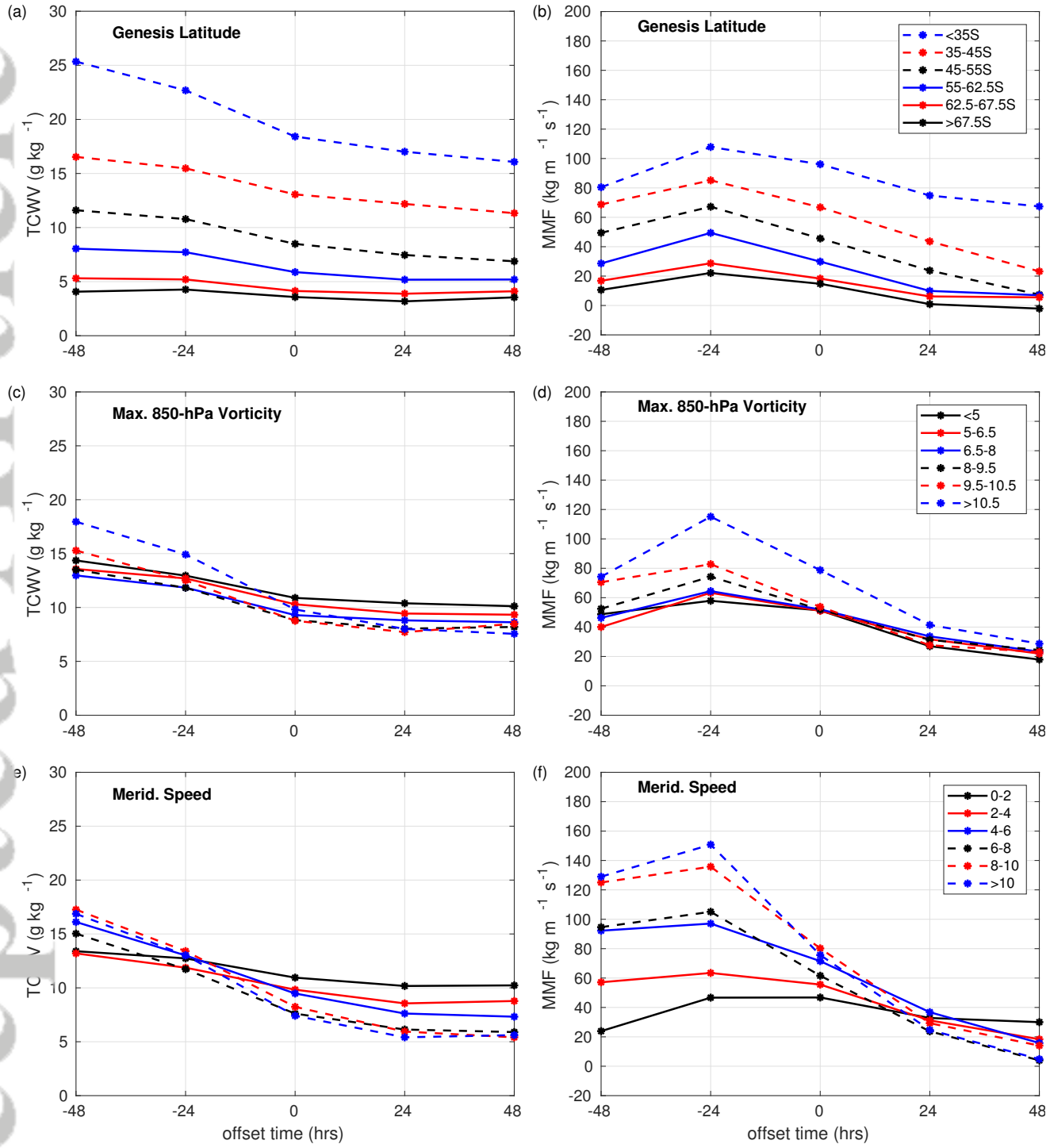


Figure 9. Mean total column water vapor (TCWV) and net vertically integrated meridional moisture flux (MMF) per unit area for cyclones in JJA as a function of time for different genesis latitude bins (a, b), different maximum vorticity bins (c,d) and different speed bins (e,f). Black solid lines: bin 1, red solid lines: bin 2, blue solid lines: bin3, black dashed lines: bin 4, red dashed lines: bin 5 and blue dashed lines: bin 6. See Table 1 for bin categories.

©2018 American Geophysical Union. All rights reserved.

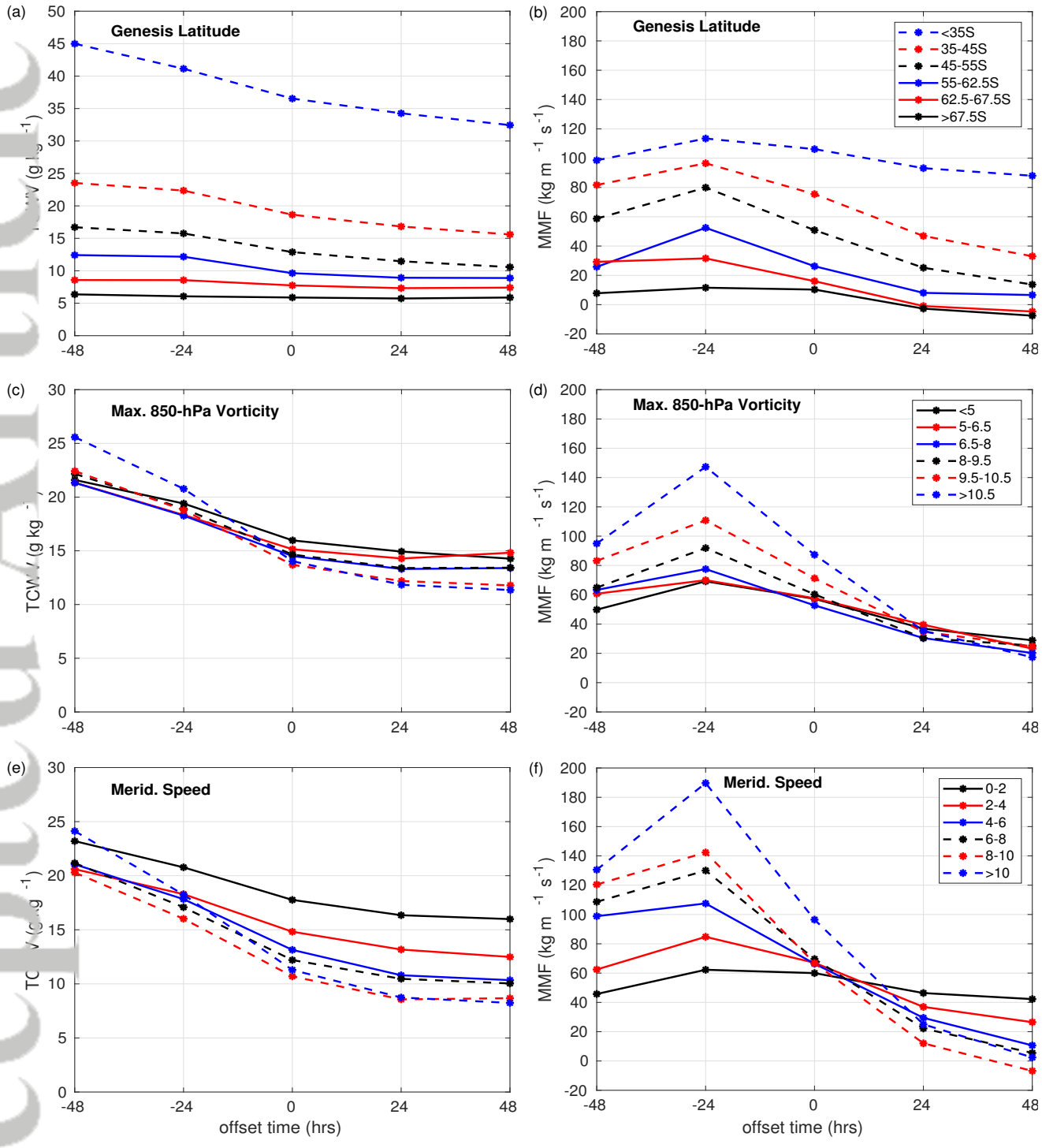


Figure 10. Storm averaged total column water vapor (TCWV) and vertically integrated meridional moisture flux (MMF) for cyclones in DJF (radius equal to 11 degrees) as a function of time for different genesis latitude bins (a, b), different maximum vorticity bins (c,d) and different speed bins (e,f). Black solid lines: bin 1, red solid lines: bin 2, blue solid lines: bin3, black dashed lines: bin 4, red dashed lines: bin 5 and blue dashed lines: bin 6. See Table 1 for bin categories.

Accepted Article

©2018 American Geophysical Union. All rights reserved.

Accepted Article

Table 4. Regression coefficients for TCVW and MMF from composite cyclones in JJA and DJF. Values in bold are statistically significant at the 99% level.

Variable	TCWV			MMF		
offset time (hr)	genesis lat	vorticity	speed	genesis lat	vorticity	speed
			JJA			
-48	**7.94**	1.34	**1.52**	**28.07**	**11.84**	**39.30**
-24	**6.95**	0.54	0.25	**33.02**	**19.73**	**39.85**
0	**5.72**	-0.49	**-1.31**	**31.22**	8.58	**11.18**
24	**5.33**	**-0.91**	**-1.78**	**27.64**	3.57	-3.17
48	**4.73**	**-0.86**	**-1.86**	**23.16**	**3.26**	**-8.16**
			DJF			
-48	**13.99**	**1.32**	-0.54	**34.76**	**15.00**	**32.48**
-24	**12.66**	0.50	**-1.07**	**38.59**	**25.52**	**44.48**
0	**11.06**	**-0.72**	**-1.01**	**37.32**	**9.19**	9.88
24	**10.25**	**-1.14**	**-0.98**	**35.54**	-1.32	**-10.09**
48	**9.46**	**-1.24**	**-0.94**	**33.32**	-2.70	**16.25**

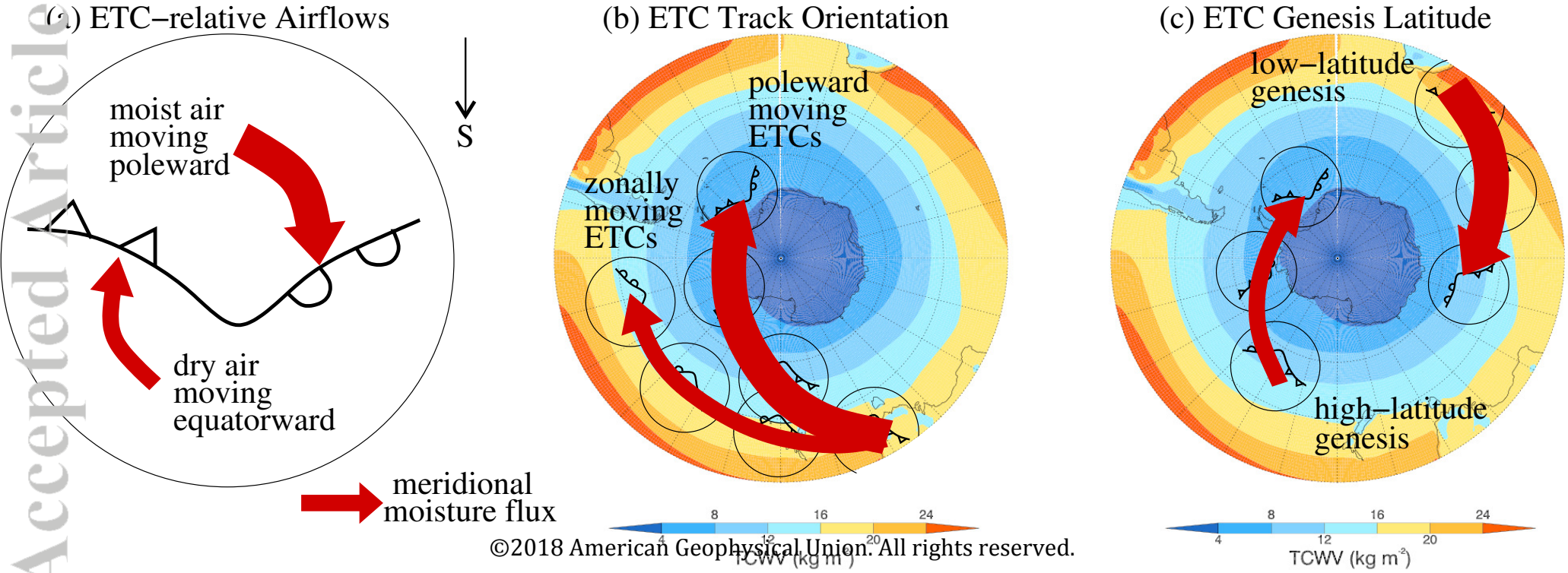
©2018 American Geophysical Union. All rights reserved.

Figure 1.

Accepted Article

©2018 American Geophysical Union. All rights reserved.

Accepted Article

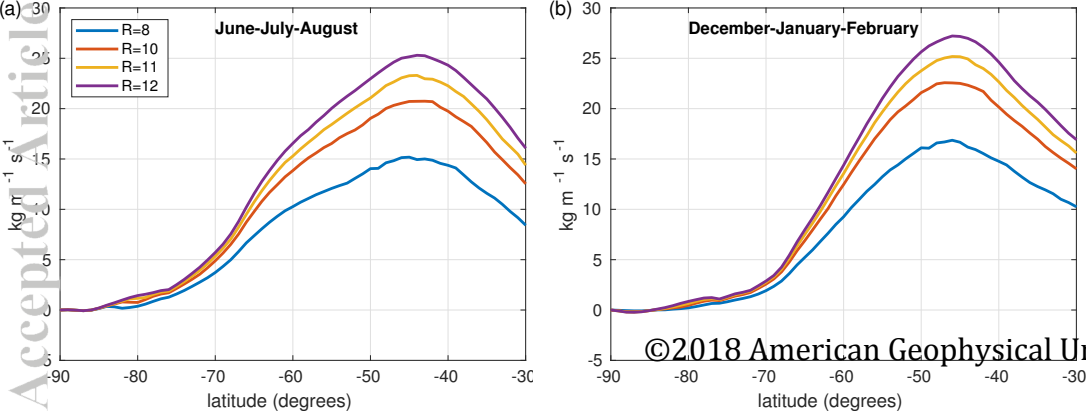


©2018 American Geophysical Union. All rights reserved.

Figure 2.

Accepted Article

©2018 American Geophysical Union. All rights reserved.

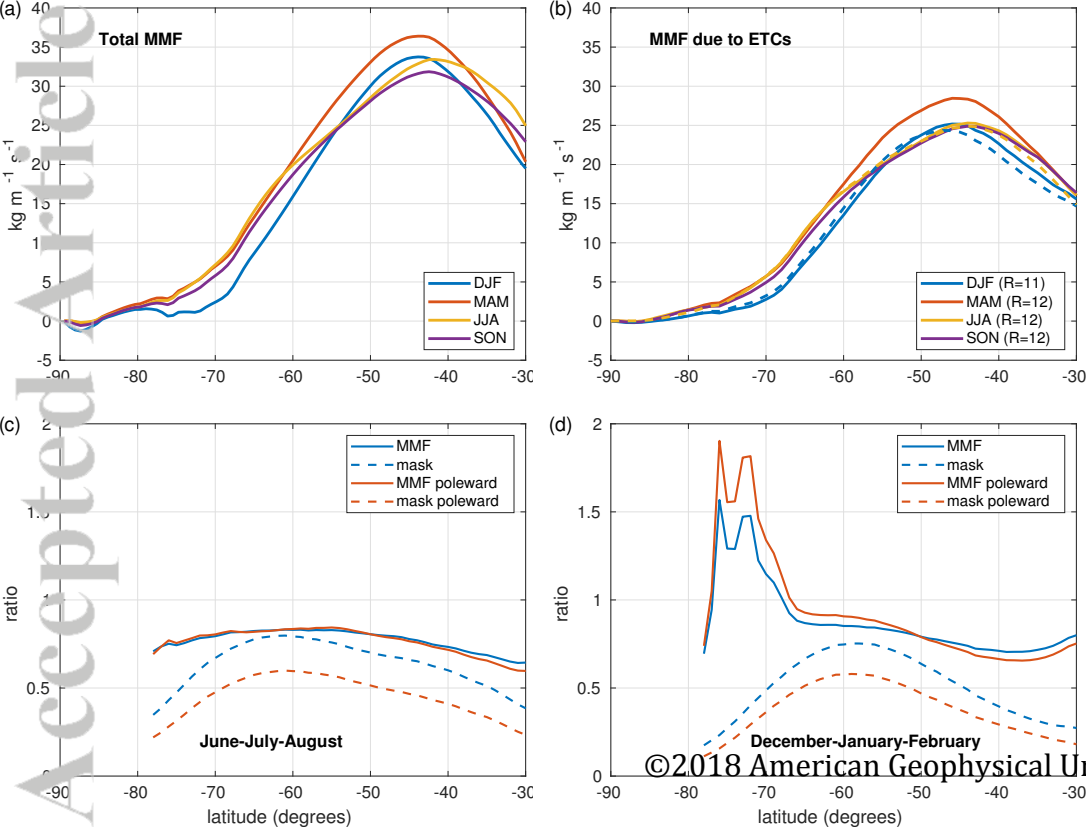


©2018 American Geophysical Un
Accepted Article

Figure 3.

Accepted Article

©2018 American Geophysical Union. All rights reserved.



Accepted Article
©2018 American Geophysical Un

Figure 4.

Accepted Article

©2018 American Geophysical Union. All rights reserved.

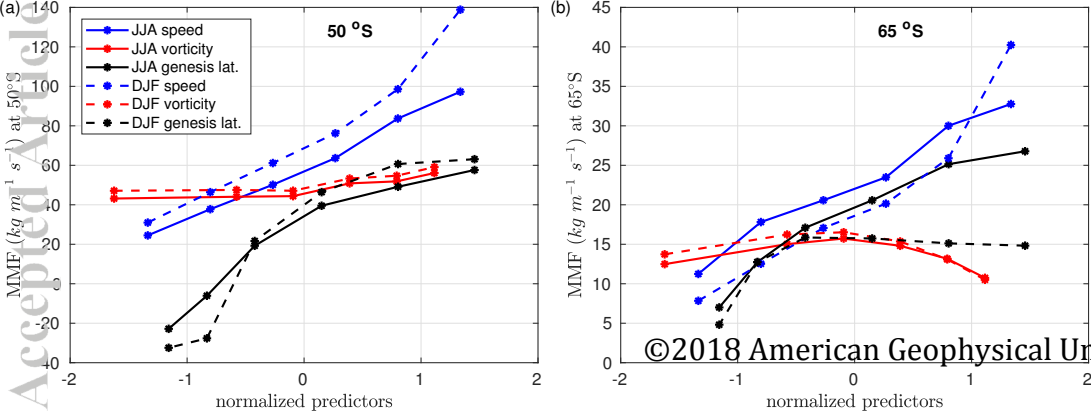
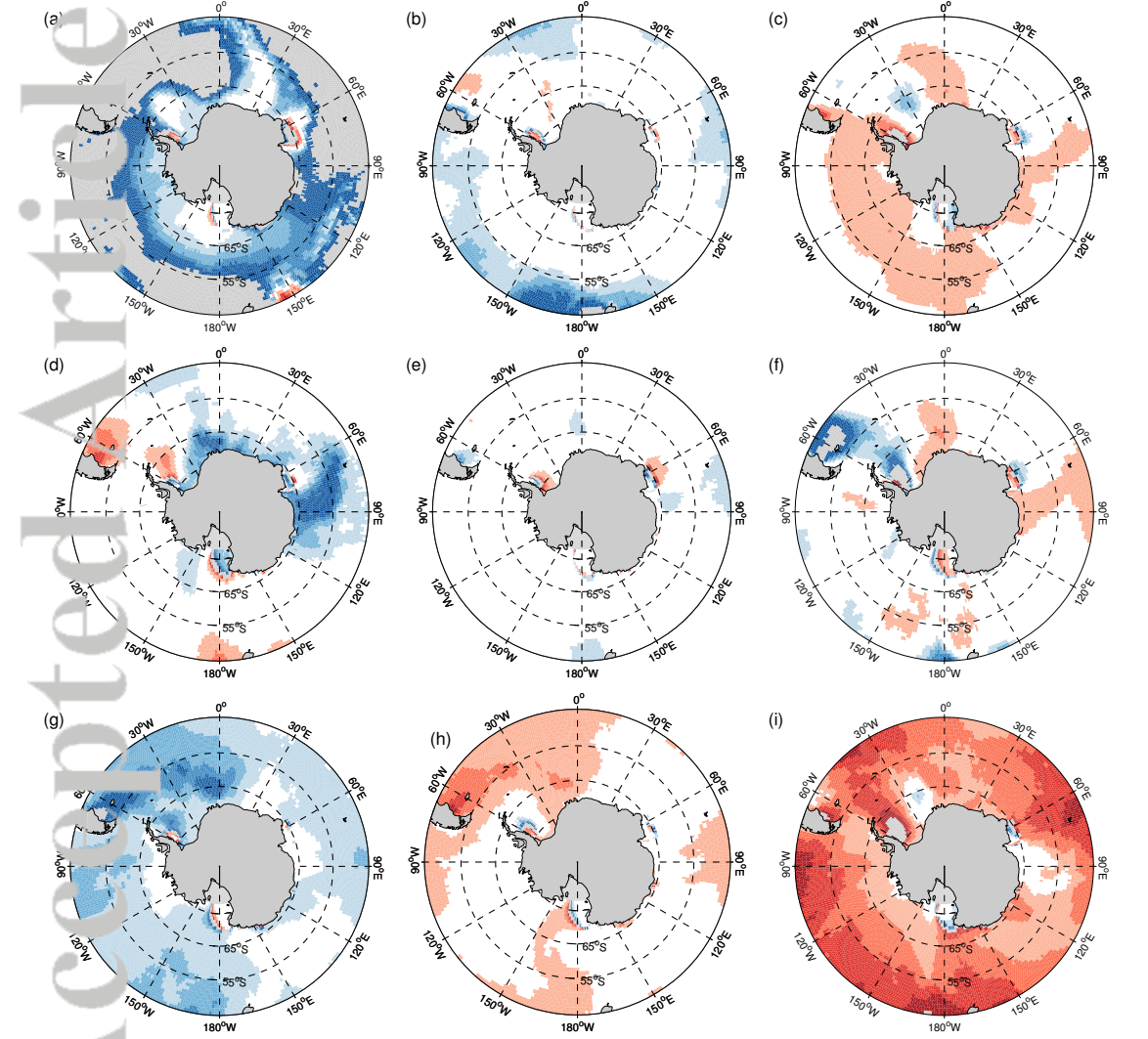

(a)
50 °S
JJA speed
JJA vorticity
JJA genesis lat.
DJF speed
DJF vorticity
DJF genesis lat.
MMF ($kg\ m^{-1}\ s^{-1}$) at 50°S
normalized predictors
(b)
65 °S
MMF ($kg\ m^{-1}\ s^{-1}$) at 65°S
normalized predictors
©2018 American Geophysical Un
Accepted Article

Figure 5.

Accepted Article

©2018 American Geophysical Union. All rights reserved.



©2018 American Geophysical Union. A

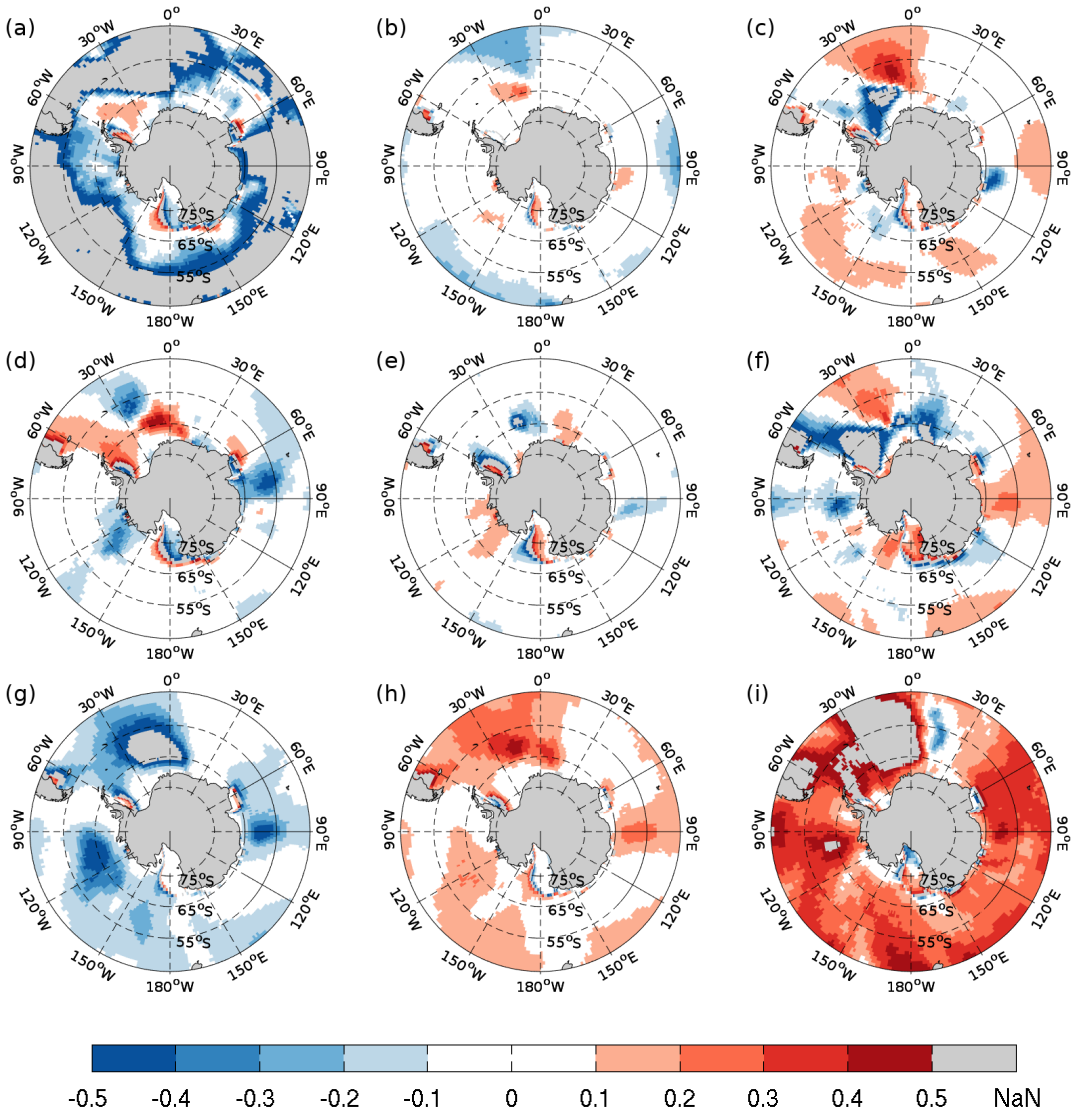
Accepted Article

Figure 6.

Accepted Article

©2018 American Geophysical Union. All rights reserved.

Accepted Article



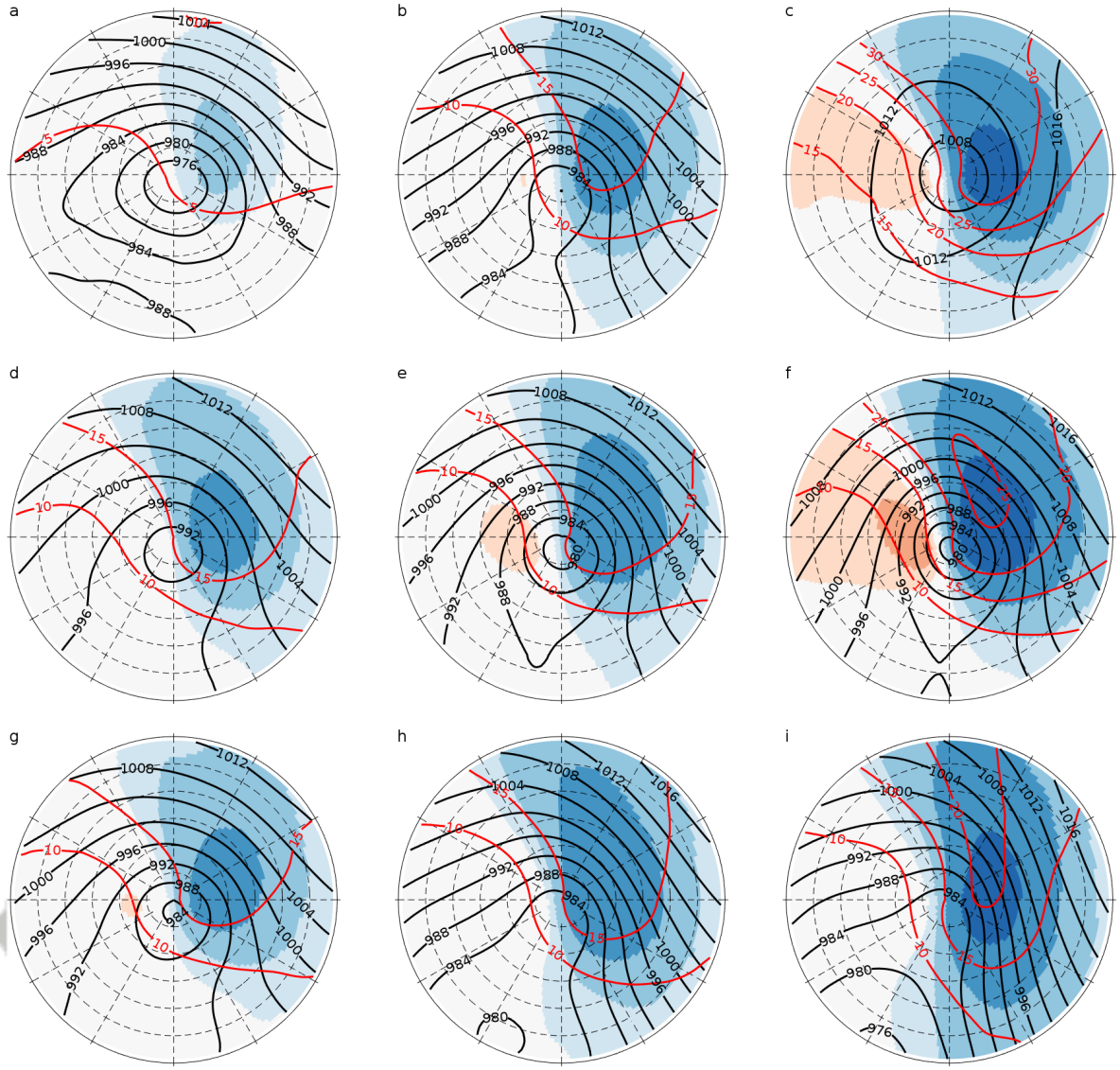
©2018 American Geophysical Union. All rights reserved.

Figure 7.

Accepted Article

©2018 American Geophysical Union. All rights reserved.

Accepted Article



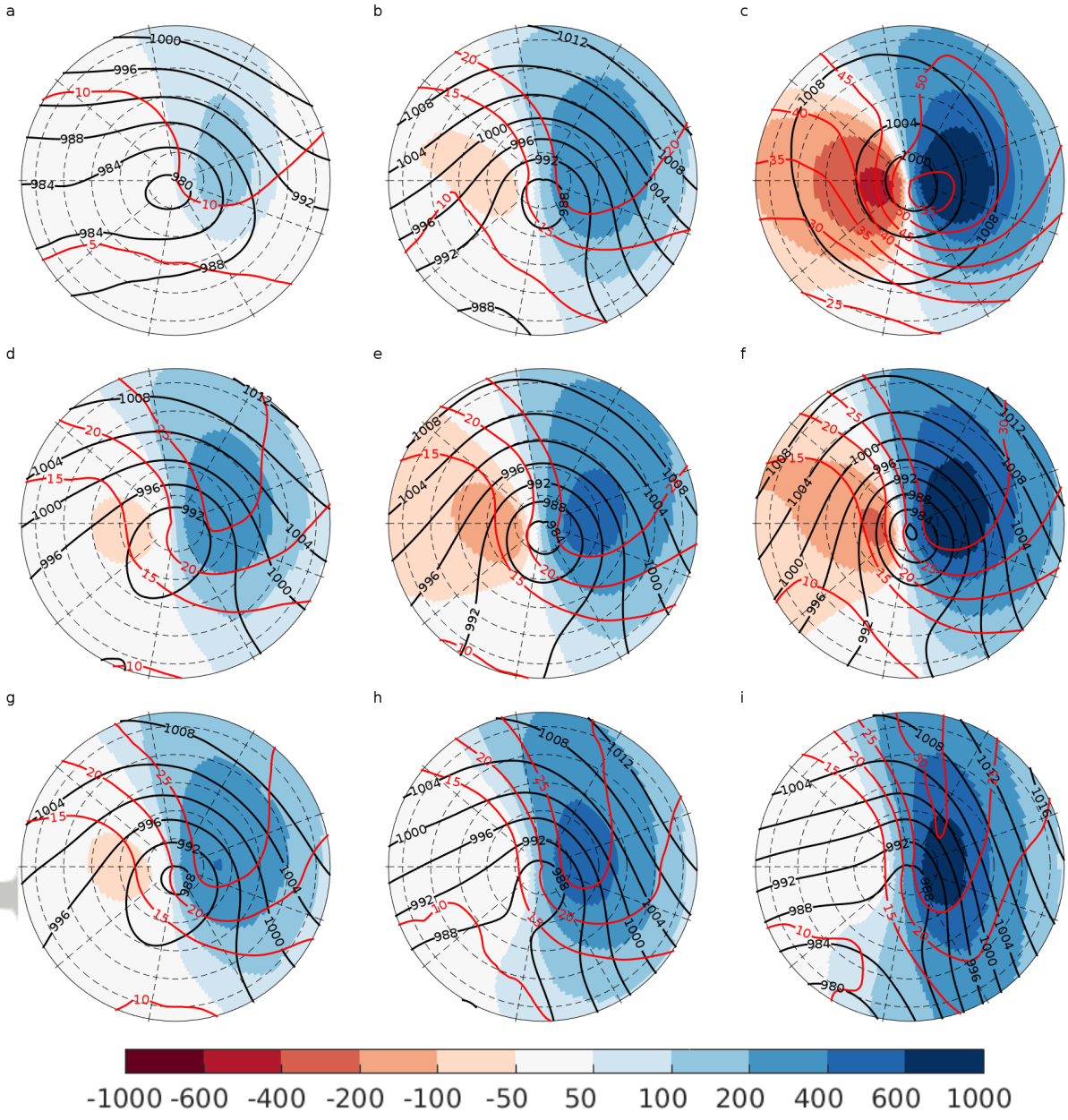
©2018 American Geophysical Union. All rights reserved.

Figure 8.

Accepted Article

©2018 American Geophysical Union. All rights reserved.

Accepted Article

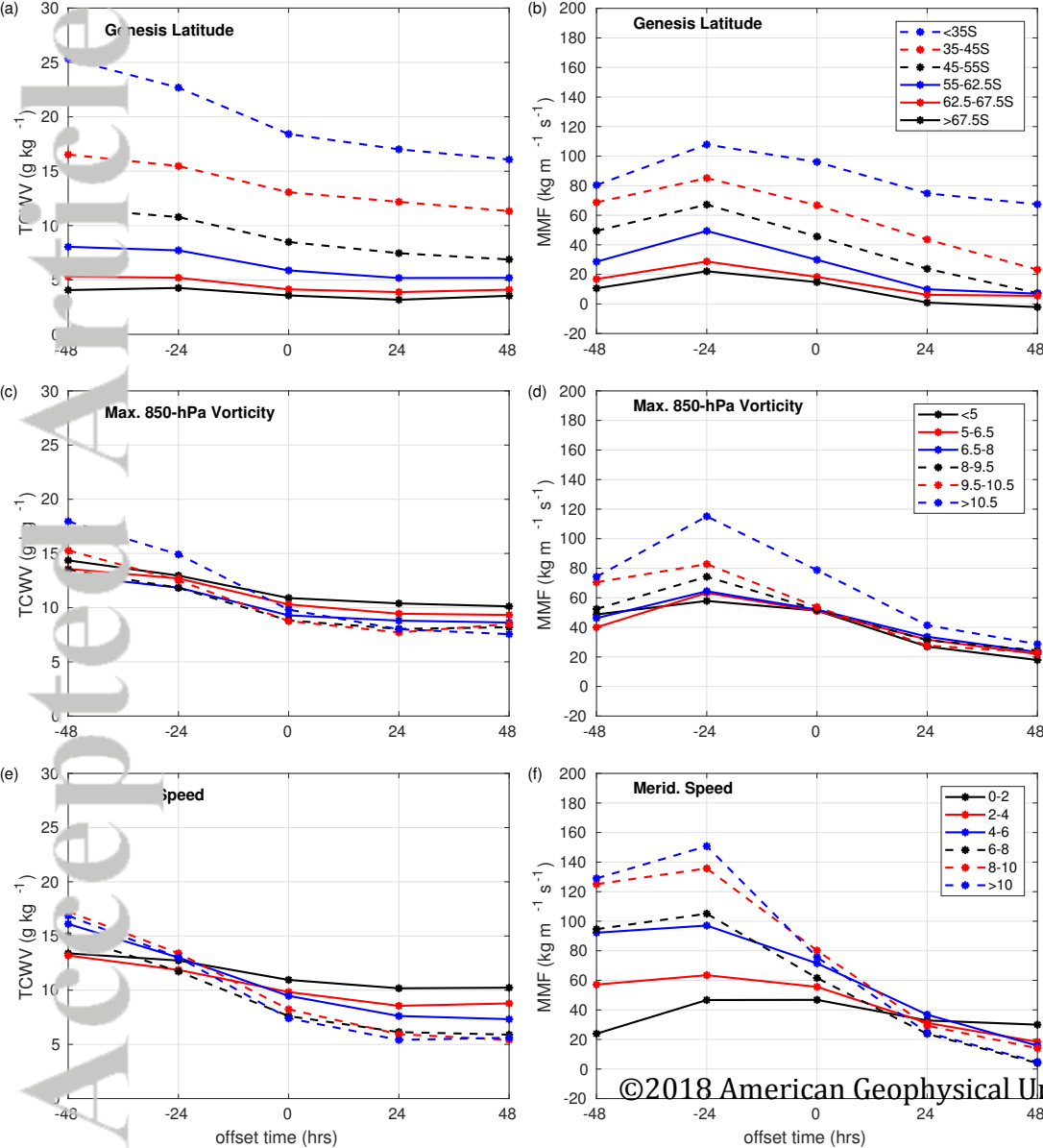


©2018 American Geophysical Union. All rights reserved.

Figure 9.

Accepted Article

©2018 American Geophysical Union. All rights reserved.



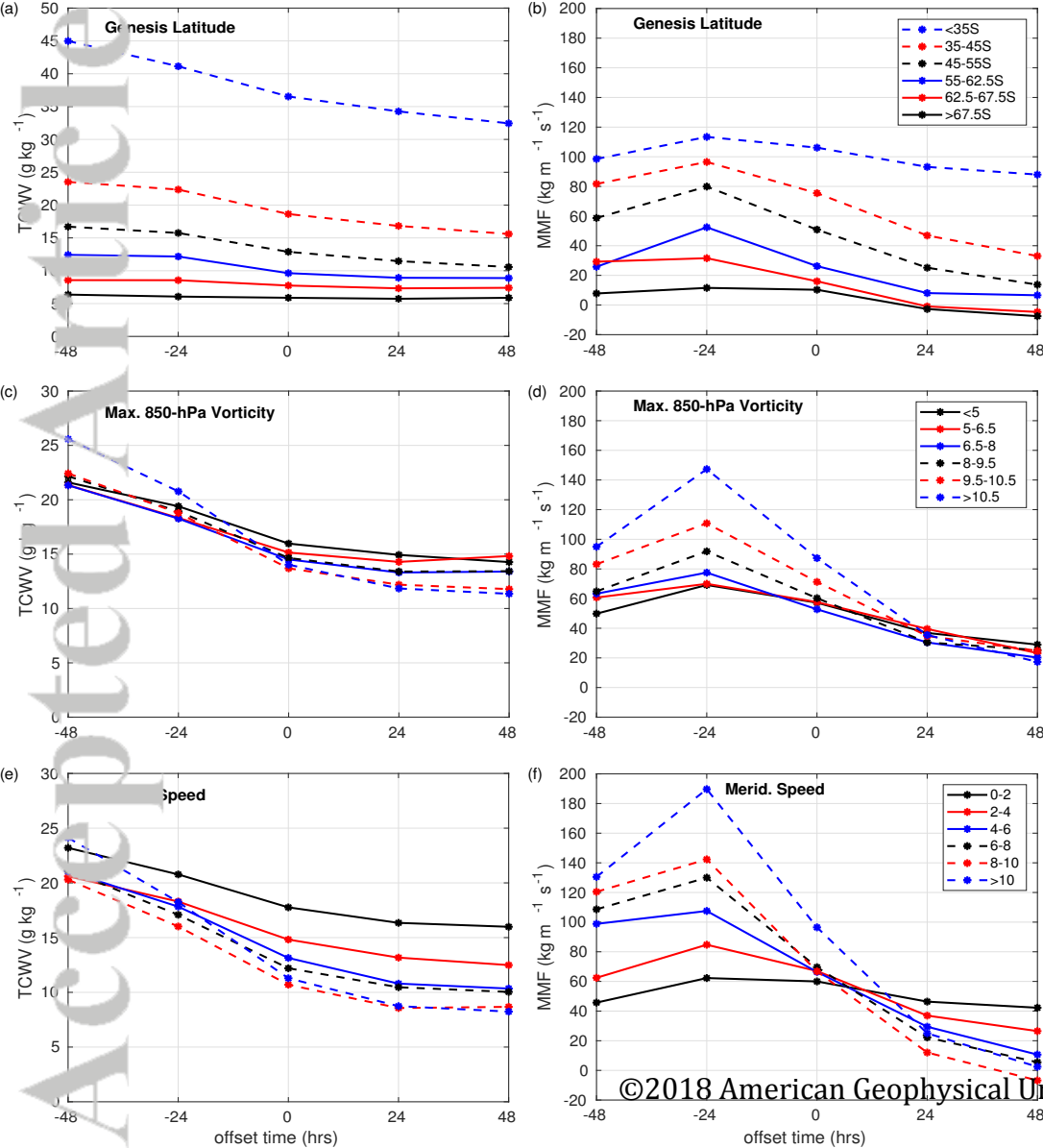
Accepted Article

©2018 American Geophysical Un

Figure 10.

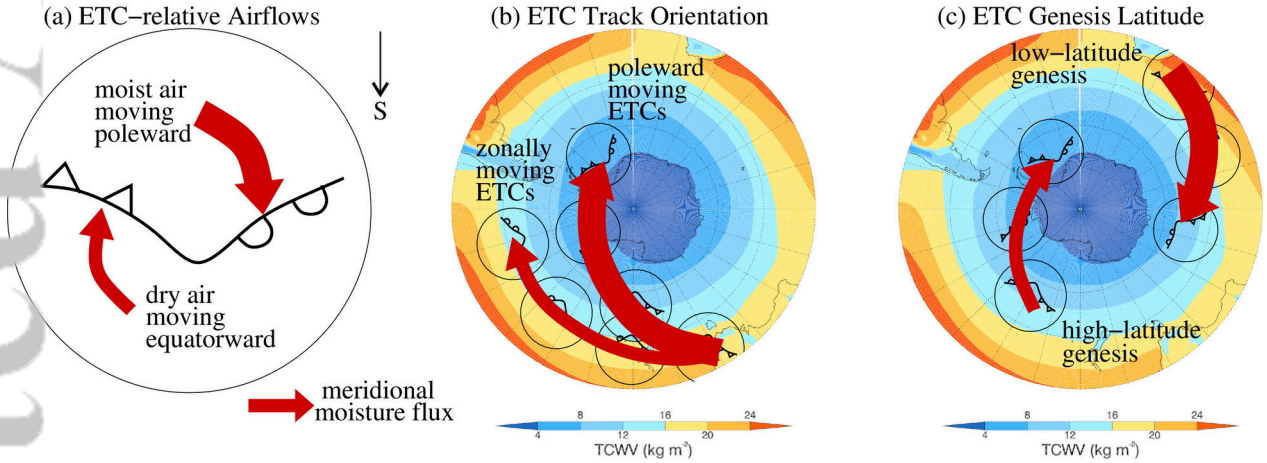
Accepted Article

©2018 American Geophysical Union. All rights reserved.



Accepted Article
©2018 American Geophysical Un

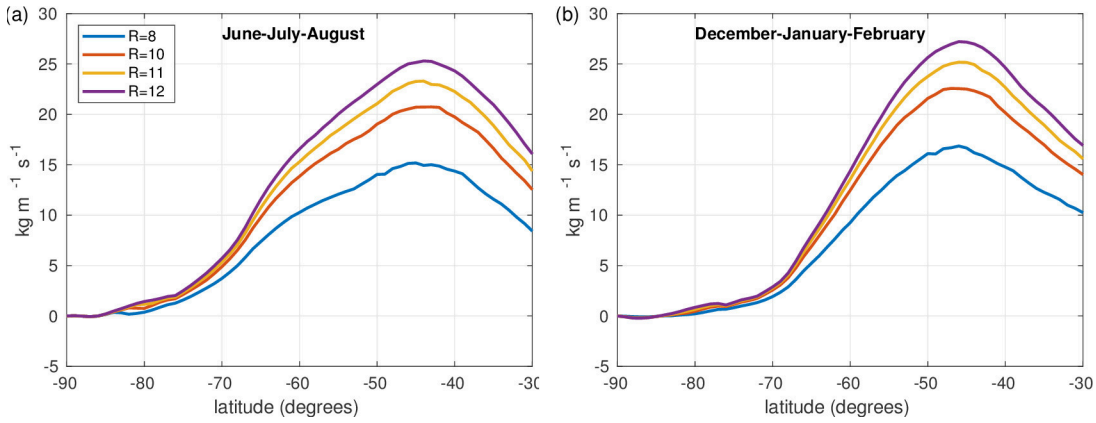
Accepted Article



2018jd028766-t-f01-z-.eps

©2018 American Geophysical Union. All rights reserved.

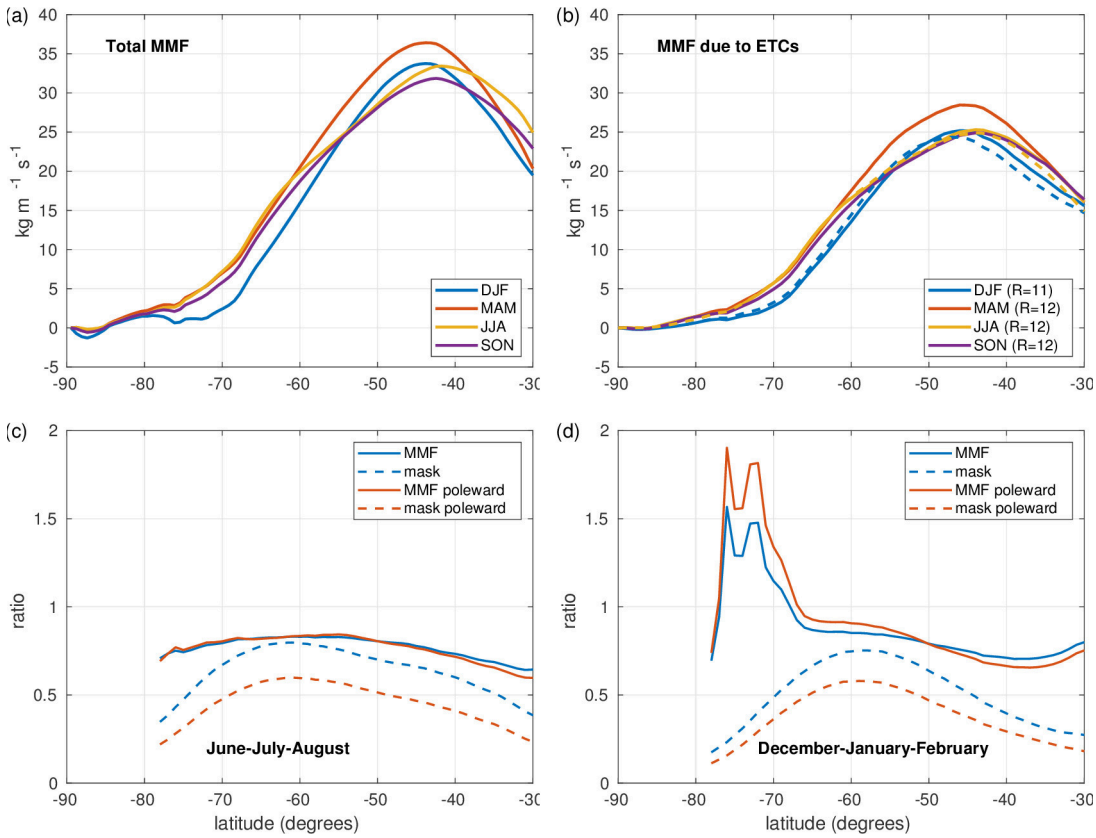
Accepted Article



2018jd028766-t-f02-z-.eps

©2018 American Geophysical Union. All rights reserved.

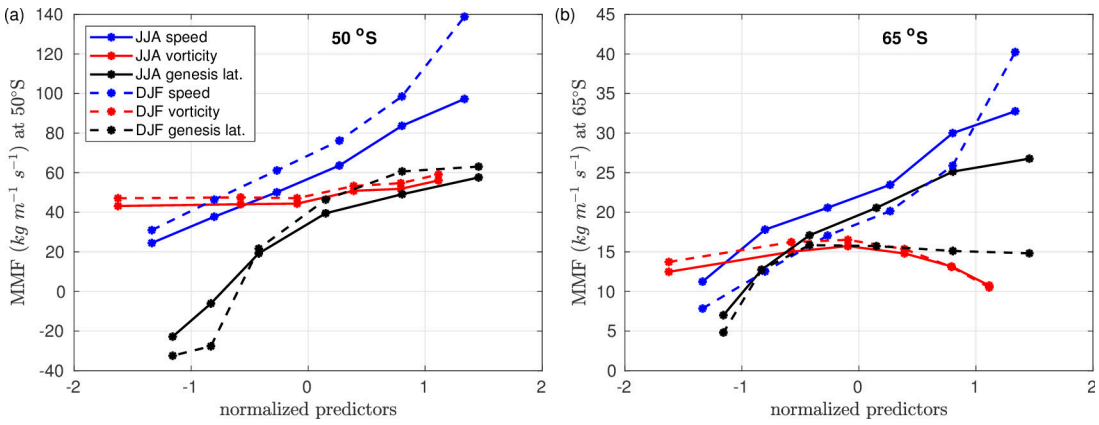
Accepted Article



2018jd028766-t-f03-z-.eps

©2018 American Geophysical Union. All rights reserved.

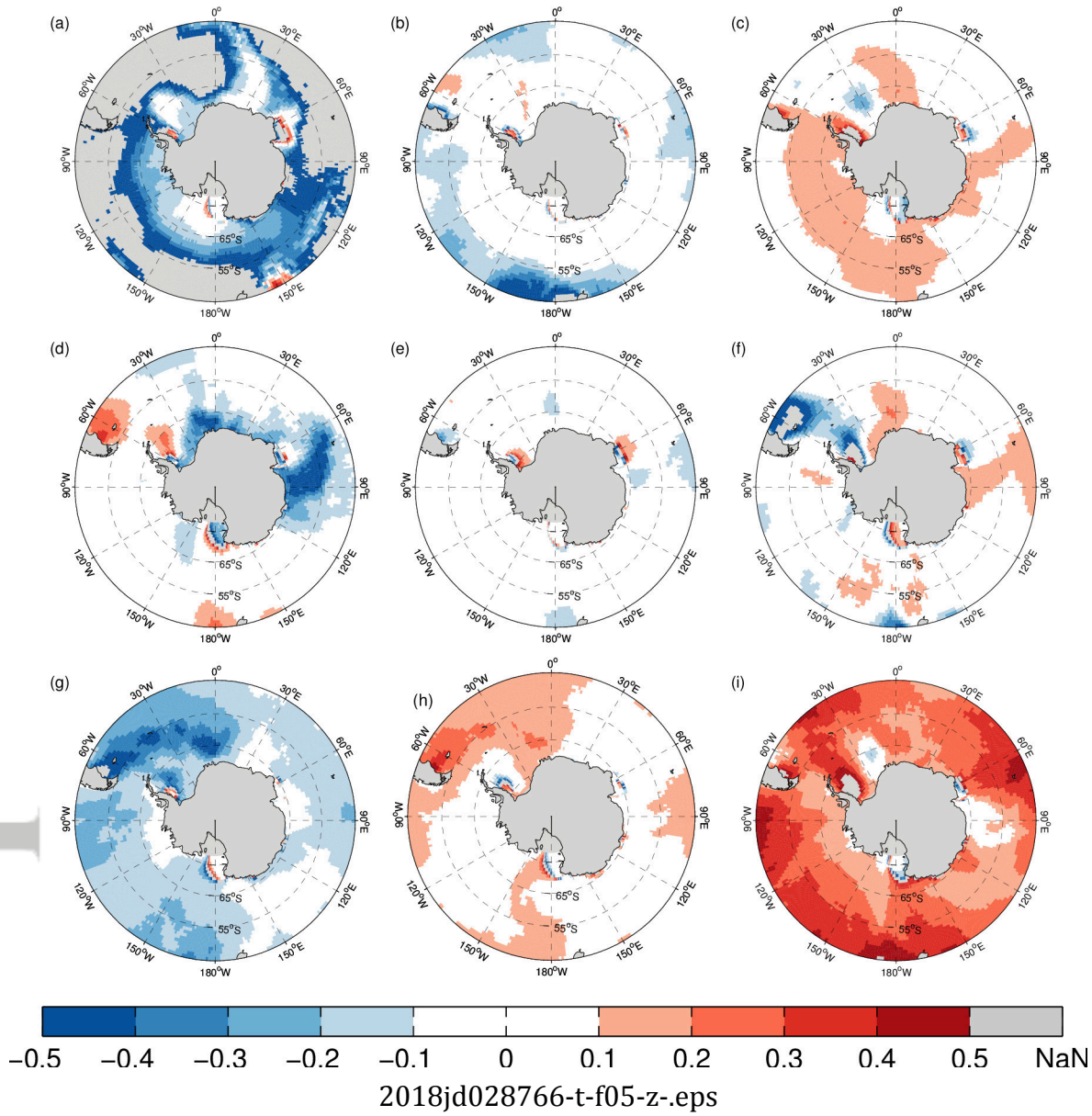
Accepted Article



2018jd028766-t-f04-z-.eps

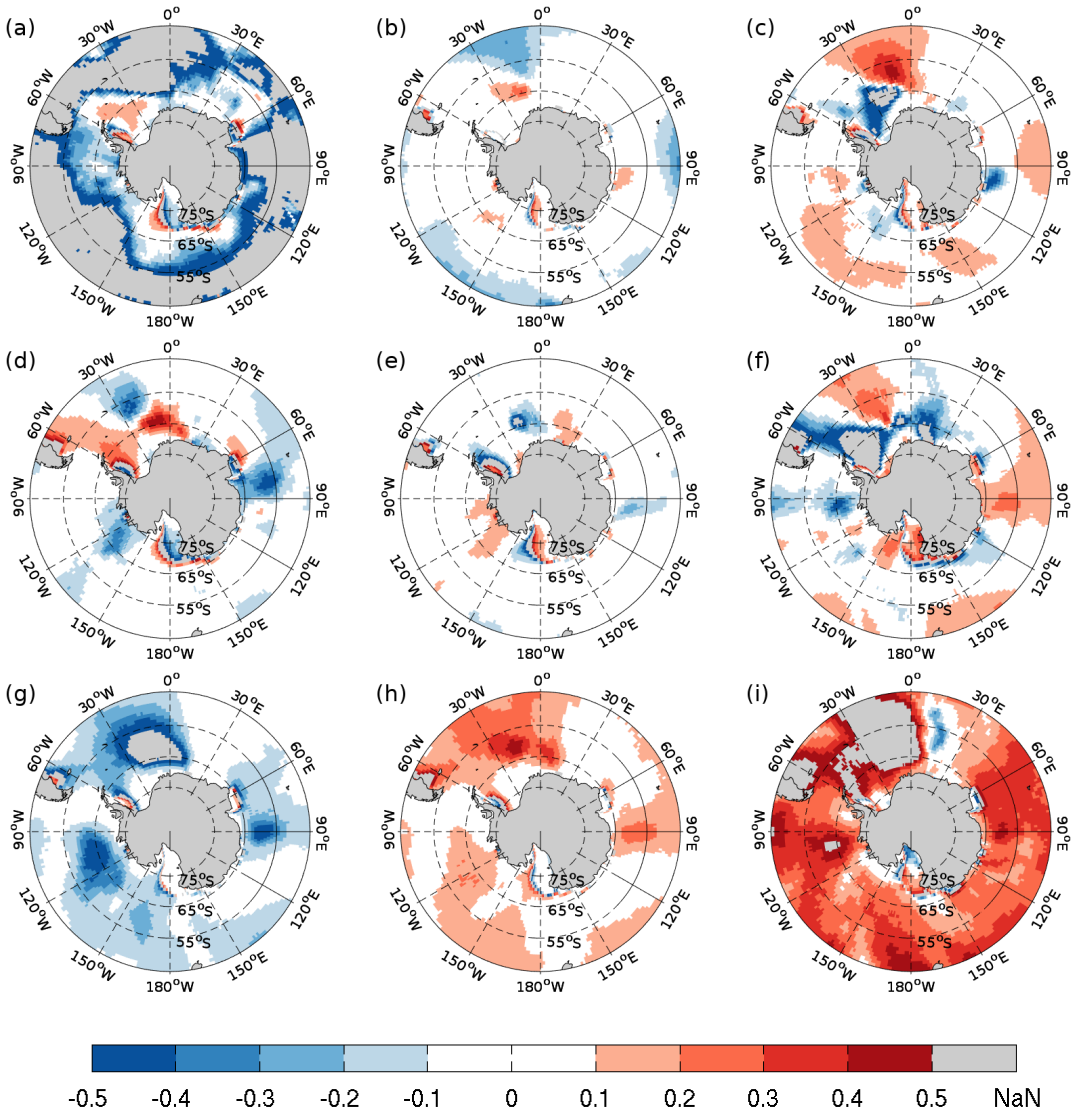
©2018 American Geophysical Union. All rights reserved.

Accepted Article



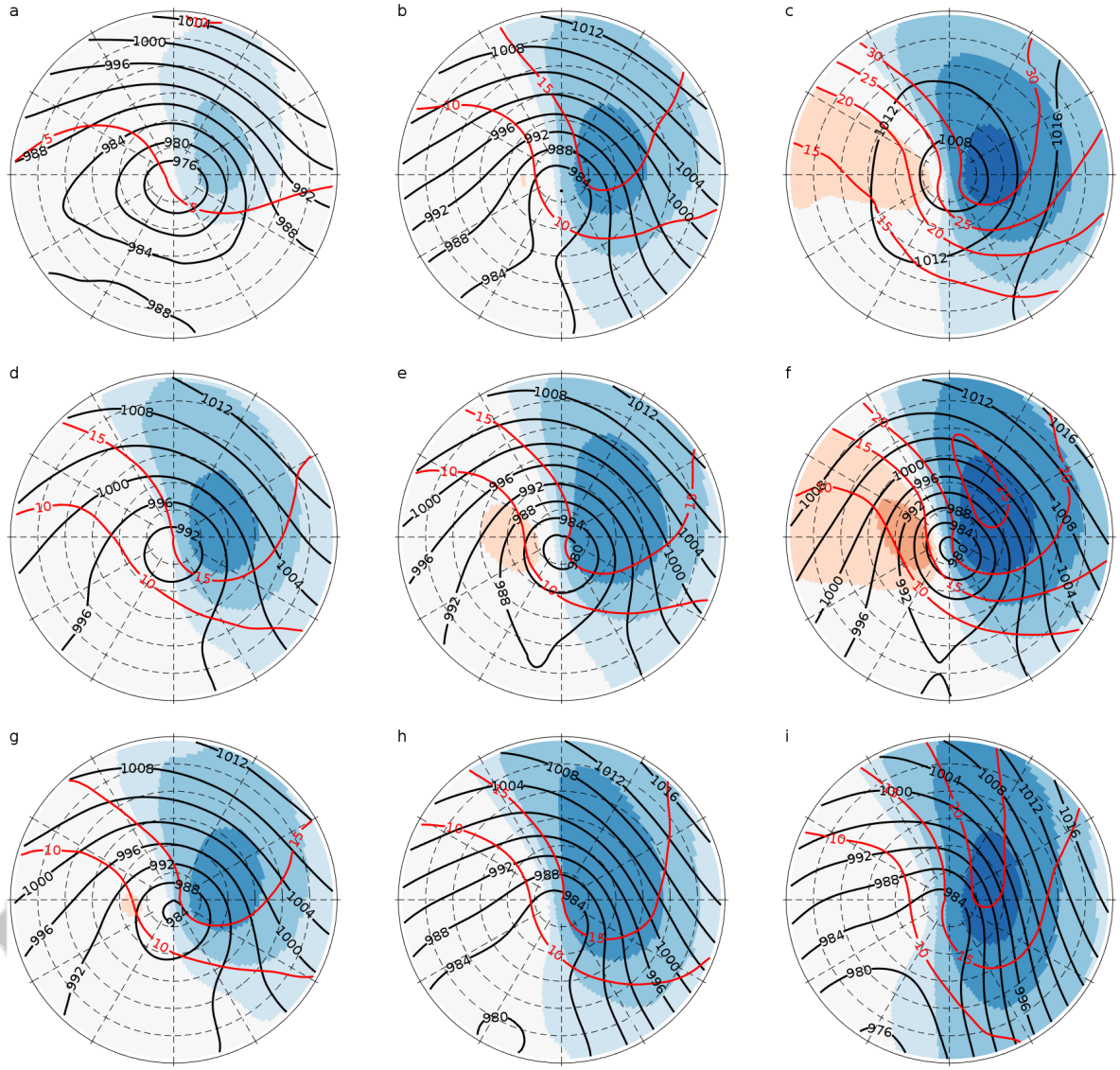
©2018 American Geophysical Union. All rights reserved.

Accepted Article



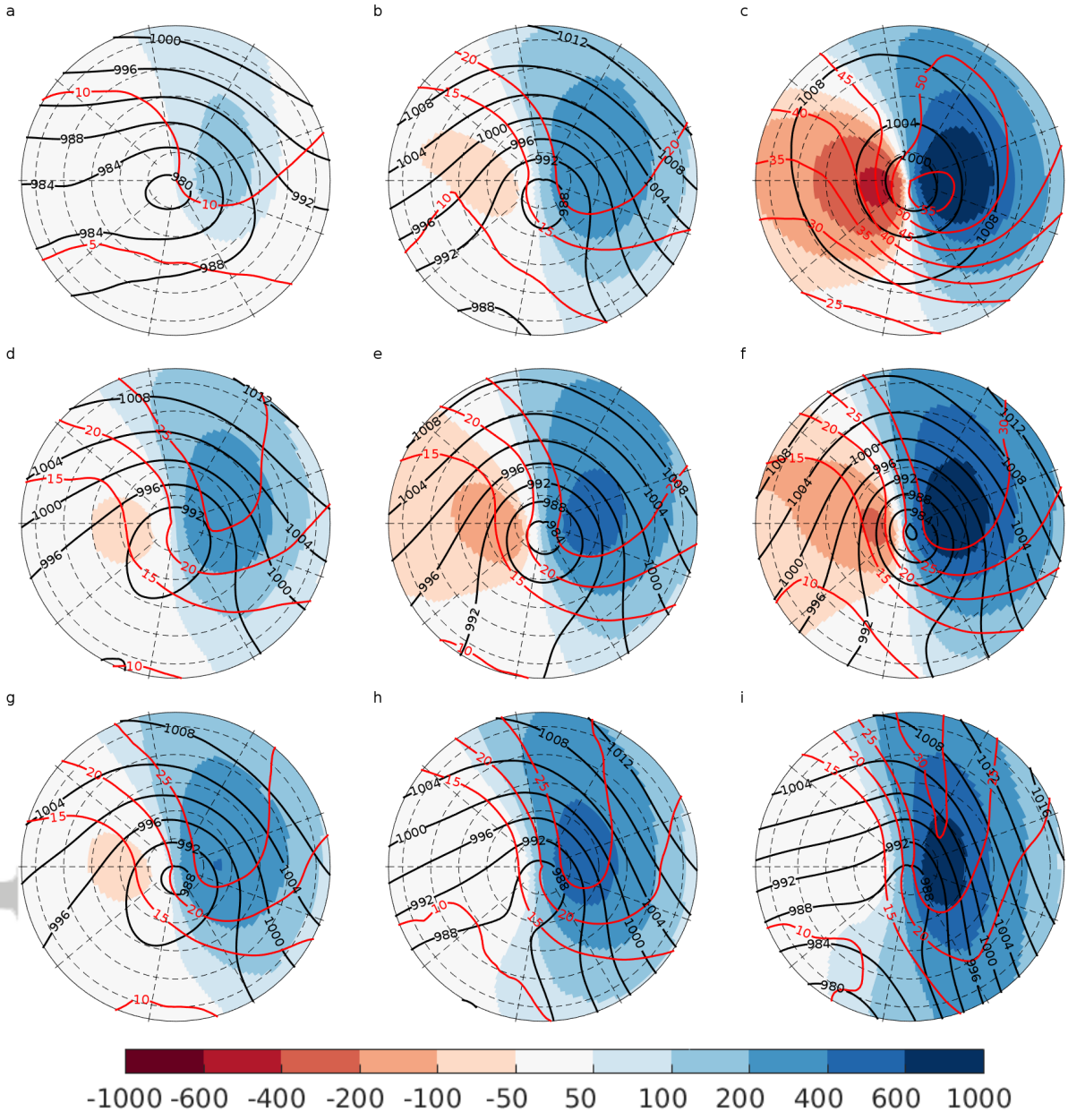
©2018 American Geophysical Union. All rights reserved.

Accepted Article



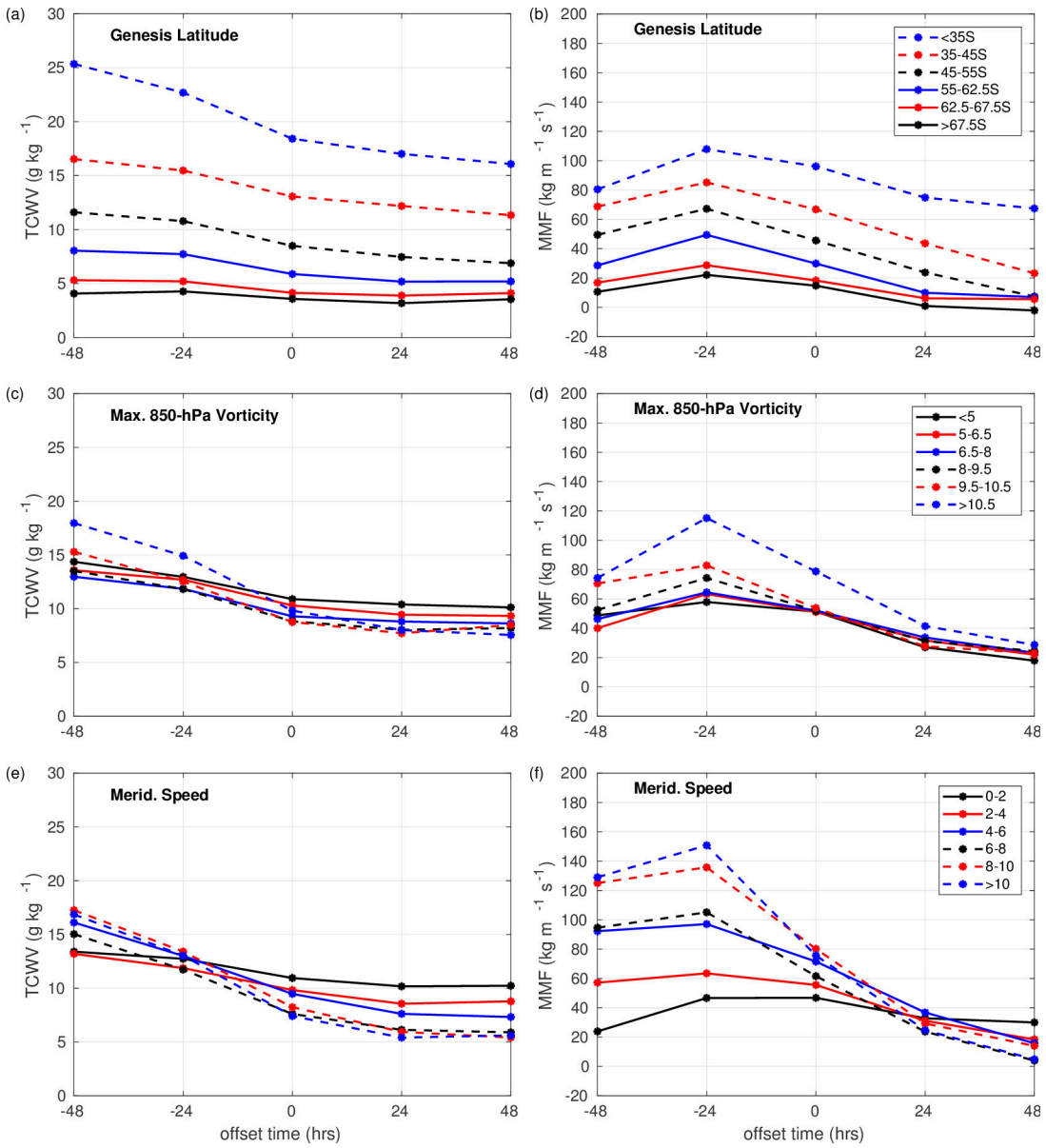
©2018 American Geophysical Union. All rights reserved.

Accepted Article



©2018 American Geophysical Union. All rights reserved.

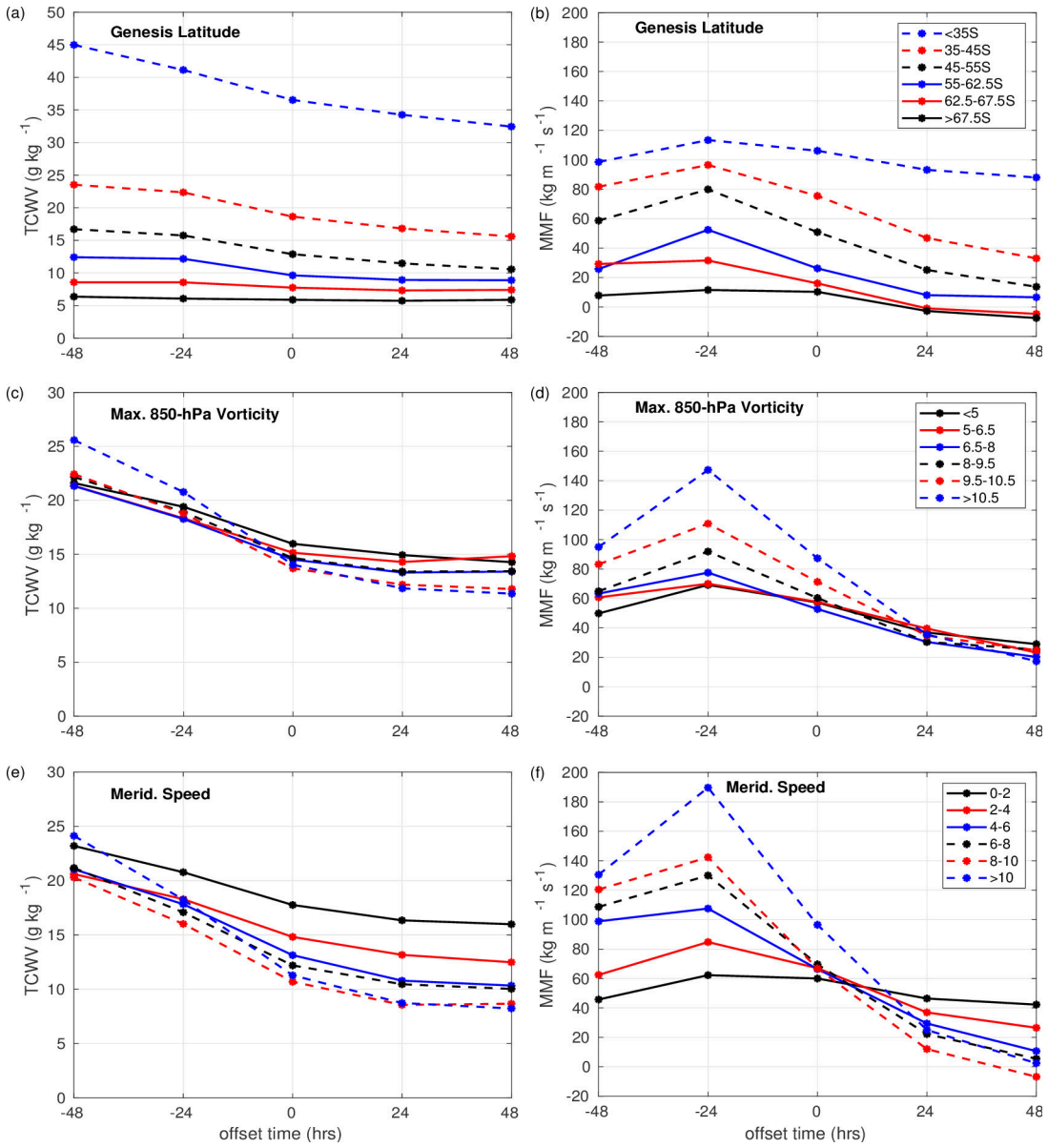
Accepted Article



2018jd028766-t-f09-z-.eps

©2018 American Geophysical Union. All rights reserved.

Accepted Article



2018jd028766-t-f10-z-.eps

©2018 American Geophysical Union. All rights reserved.